International Journal of Mechanical Sciences 69 (2013) 94–106

Contents lists available at SciVerse ScienceDirect

International Journal of Mechanical Sciences

journal homepage: www.elsevier.com/locate/ijmecsci

Large deflection thermoelastic analysis of functionally graded stiffened annular sector plates

M.E. Golmakani [a], M. Kadkhodayan [b,*]

[a] Department of Mechanical Engineering, Mashhad Branch, Islamic Azad University, Mashhad, Iran
[b] Department of Mechanical Engineering, Ferdowsi University of Mashhad, Mashhad 91775-1111, Iran

ARTICLE INFO

Article history:
Received 26 June 2012
Received in revised form
29 November 2012
Accepted 26 January 2013
Available online 13 February 2013

Keywords:
Large deflection
Stiffened FG sector plates
Thermoelastic analysis
DR method

ABSTRACT

In this study the large deflection behaviors of stiffened annular functionally graded (FG) sector plates under mechanical and thermo-mechanical loadings with various boundary conditions are investigated. Material properties are assumed to be graded in the thickness direction according to a simple power law distribution in terms of the volume fractions of the constituents. Based on first-order shear deformation plate theory (FSDT) and von Karman relations for large deflection, nonlinear equilibrium equations are developed. Dynamic relaxation (DR) numerical method combined with the finite difference discretization technique is used to solve the plate nonlinear equations. Effects of material grading index, boundary condition, stiffener depth to the plate thickness ratio and thermal gradient are discussed.

1. Introduction

In order to achieve greater structural efficiency and material economy, stiffened plates are sometimes used in place of uniform thickness plates. The design of the former plate category is, however, more complicated [1]. Stiffened plates are employed in a wide variety of structures, e.g. steel bridges, offshore platforms, ship hulls and aircraft wings. Over many decades design and research engineers have demonstrated great skill in developing and understanding of the response of stiffened plates to various loading arrangements, especially transverse pressure and uniform in-plane compression, and in formulating practical rules and guidance for their safe and economic design [2]. From the analysis stance, stiffened sector plates may be studied as equivalent anisotropic uniform thickness plates providing the number of stiffeners is large. According to this approach, research effort is centered on the transformation of the structural orthotropy to equivalent material orthotropy [3]. For practical and economic reasons, small numbers of stiffeners are generally used to stiffened plates [4]. Thus, the first approach is not under investigation here. Instead, attention is focused on sector plates stiffened by a single eccentric radial stiffener. In the second approach, valid when only a few stiffeners are presented, the plate and stiffeners are treated as separate entities and kinematic continuity and force interaction at the plate-stiffener junctions is enforced [3]. One such theory that has been developed for discretely stiffened rectangular plate is due to Basu et al. [5]. Both approaches are explained in detail in Troitsky's classic text [6]. Application of the latter approach to large deflection response was much more difficult. Although the flexibility, validity and accuracy inherent in this type of stiffened plate model are less than that it may be expected from say a finite element model in which both the plate and the stiffener are treated as plate, the former model is of value because of the computational and formulation benefits that arise [2]. Several years ago, Turvey [7] developed a discretely stiffened circular plate analysis and applied it to the elastic large deflection analysis of ring-stiffened circular composite plates. A similar analysis was also used by Turvey and Der Avanessian [8,9] to investigate the effect of ring-stiffener depth on the elastic and elasto-plastic large deflection response of steel plates. Turvey and Salehi [3,4] used a finite-difference implementation of the dynamic relaxation (DR) algorithm to analyze non-axisymmetric elastic large deflection of solid and annular thin sector plates stiffened by a single eccentric rectangular cross-section radial stiffener. Using the similar method, Turvey and Salehi [1] also solved the governing equations for the elastic large deflection of uniformly pressure loaded axisymmetric discretely stiffened isotropic circular plates based on the classical plate theory (CPT). To the knowledge of the authors', there is no literature regarding the nonlinear response of an eccentrically stiffened annular functionally graded sector plate under mechanical and thermo-mechanical loading, based on first order shear deformation plate theory (FSDT). The functionally graded materials (FGMs) were initially designed in 1984 by a group of material scientists in Japan, as thermal barrier materials for aerospace structural applications and fusion reactors [10,11], and nowadays are

* Corresponding author.
E-mail addresses: m.e.golmakani@mshdiau.ac.ir (M.E. Golmakani), kadkhoda@um.ac.ir (M. Kadkhodayan).

0020-7403/$ - see front matter © 2013 Elsevier Ltd. All rights reserved.
http://dx.doi.org/10.1016/j.ijmecsci.2013.01.033

developed for a more general use as structural components in extremely high-temperature environments [12]. Typically these materials are made from a mixture of ceramic and metal in which the ceramic component provides high-temperature resistance due to its low thermal conductivity; on the other hand, the ductile metal component prevents fracture caused by thermal or mechanical stresses. Some analytical studies have been considered static small deflection analysis of functionally graded sector plates [13–16]. With the introduction of digital computers, numerical methods become very popular in engineering application and several different techniques have been used for solving very complicated problems, namely dynamic relaxation [1–4], finite element (FEM) [17–24], etc. Using smoothed finite element method, Nguyen-Xuan et al. [17–24] investigated static, free vibration and buckling analysis of isotropic, laminated and functionally graded plate/shell based on Reissner/Mindlin theory and higher-order shear deformation plate theory (HSDT). In their studies [17–24], in order to avoid the transverse shear locking and to improve the accuracy of the formulation, the edge/node-based smoothed finite element method (ES/NS-FEM) was incorporated with stabilized discrete shear gap (DSG) technique. Numerical results of the mentioned studies show that the proposed approaches are robust, computational inexpensive and simultaneously very accurate and free of locking. Moreover, novel approaches were proposed by others [25–27] on solution accuracy of FEM within the isogeometric analysis using a generalization of NURBS enabling local refinement and polynomial splines over hierarchical T-meshes (PHT-splines). To the best of authors' knowledge, no work has been reported concerned with the small and large deflection analysis of eccentrically stiffened annular FG sector plates under mechanical and thermo-mechanical loading. Hence, the present paper is concerned with a further development of the discretely stiffened isotropic sector plate analysis used in Refs. [3,4], for the thermo-elastic large deflection response of FG annular sector plates with discrete radial stiffeners based on FSDT. The material properties of the FG sector plates are assumed to vary continuously through the thickness of the plate according to the simple rule of mixture. The plate is subjected to a uniform pressure loading in thermal environments and the boundary conditions are simply supported and clamped. In this work, details of the FG sector plates stiffened by a single eccentric rectangular cross-sectional radial stiffener under consideration are introduced first. Thereafter, the governing stiffened FG plate equations are introduced and the modeling of the interaction between the stiffener and the plate is explained. The force interaction is complemented with a set of plate-stiffener displacement compatibility equations. An explanation of the transformation of these equations for subsequent numerical solution with the dynamic relaxation (DR) algorithm is then given. The validation of the DR solutions by comparison with corresponding results for isotropic materials [3] is described next and this is followed by the main parameter study results. The latter numerical results are presented to show the effect on deflections, stress resultants and stress couples of material composition, temperature rise, boundary conditions, stiffener depth and plate thickness ratio.

2. Plate and stiffener details

Fig. 1 shows the stiffened annular FG sector plate geometry with the thickness, sector angle, inner and outer radiuses of h, α, r_i and r_0, respectively, subjected to a transverse uniform loading q and thermal gradient ΔT through the thickness in the orthogonal polar coordinate system r, θ, z. The FG sector plate is stiffened on one face by a single diametral isotropic stiffener of rectangular

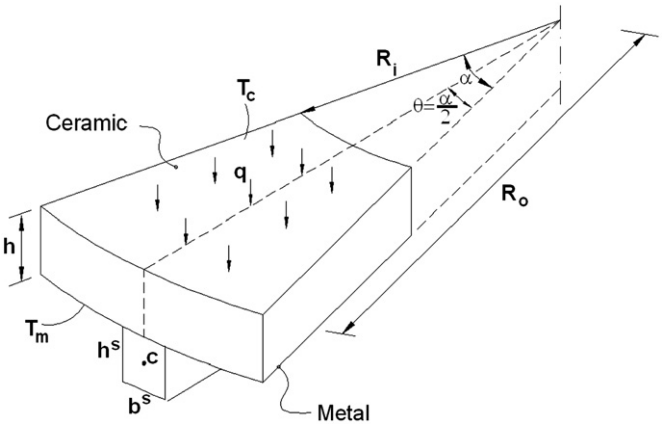

Fig. 1. The eccentrically stiffened annular FG sector plate geometry under thermo-mechanical loading.

cross section. The width of the stiffener is b^s and its depth is h^s (see Fig. 1). It is assumed that the plate and stiffener are made of FGMs and isotropic elastic material, respectively. An FGM is typically made from a mixture of ceramics and metal with a continuously varying volume fraction throughout the thickness of plate. Some models in the literature express the variation in the mechanical and thermal properties in the FGMs. The most commonly used model is the power law distribution of the volume fraction. According to this model, the composition is normally considered to vary from upper to the lower surface of the plate such that the top surface ($z=h/2$) is ceramic-rich, whereas the bottom surface ($z=-h/2$) is metal-rich. The effective material properties P can be expressed as

$$P = P_c V_c + P_m V_m, \tag{1}$$

where subscripts m and c denote the metallic and ceramic constituents, respectively; V_c and V_m are the ceramic and metal volume fractions, respectively, and are related by

$$V_c + V_m = 1 \tag{2}$$

The ceramic volume fraction V_c is assumed to follow a power law distribution as

$$V_c = \left(\frac{2z+h}{2h}\right)^n, \tag{3}$$

where z is the thickness coordinate ($-h/2 \le z \le h/2$) and volume fraction index n dictates the material variation profile through the plate thickness and can be varied to get the optimum distribution of component materials. This study assumes Poisson's ratio υ to be constant and the elastic modulus E, thermal conductivity K and thermal coefficient of expansion α to vary according to the gradation relation in Eq. (1). By substituting Eq. (1) into Eq. (2), the material properties of the FGM plate are determined as

$$\begin{cases} E(z) = (E_c - E_m)\left(\frac{2z+h}{2h}\right)^n + E_m, \\ \alpha(z) = (\alpha_c - \alpha_m)\left(\frac{2z+h}{2h}\right)^n + \alpha_m, \\ K(z) = (K_c - K_m)\left(\frac{2z+h}{2h}\right)^n + K_m. \end{cases} \tag{4}$$

The elastic characteristics of the isotropic stiffener are also as the same as the metallic phase of FG sector plate. It is convenient to organize the geometric variables, which define the stiffened plate, into a number of dimensionless groups. These are: (1) the plate thickness to radius ratio $\mu = h_0/r_0$, (2) the stiffener depth to plate thickness ratio $\xi = h^s/h_0$, (3) the stiffener width to plate thickness ratio$\eta = b^s/h_0$ and (4) the sector angle α.

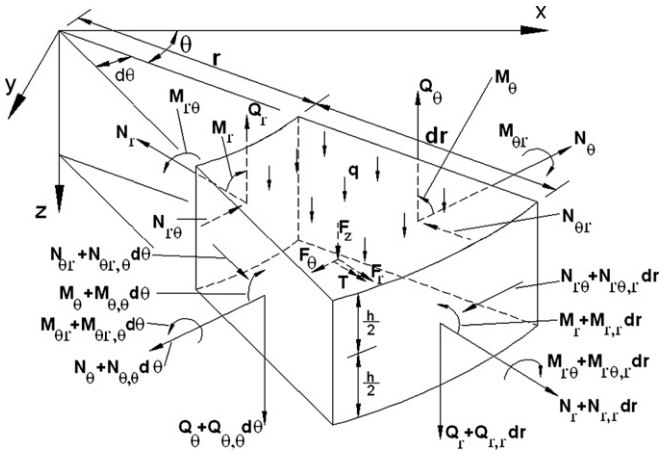

Fig. 2. Free diagram of the stiffened annular sector plate.

3. Governing plate and stiffener equations

The large deflection stiffened FG sector plate equilibrium equations were derived by considering the equilibrium of the internal stress resultants and stress couples, the external pressure and the interaction forces and couples between the plate and the stiffener acting on small elements of the plate and stiffener (see Fig. 2). Here, in the interests of brevity, only the final forms of the equilibrium equations are presented.

3.1. Sector plate equations

Fig. 2 shows the internal and external forces and moments acting on the cross section areas of the annular FG sector plate. The in and out-of-plane force and moments equilibrium equations along the radial and circumferential direction based on FSDT take the following forms:

$$\begin{cases} \frac{\partial N_r}{\partial r}+\frac{1}{r}\frac{\partial N_{r\theta}}{\partial \theta}+\frac{1}{r}(N_r-N_\theta)+\underline{\frac{F_r}{r\Delta\theta}}=0, \\ \frac{\partial N_{r\theta}}{\partial r}+\frac{1}{r}\frac{\partial N_\theta}{\partial \theta}+\frac{2}{r}N_{r\theta}+\underline{\frac{F_\theta}{\Delta r}}=0, \\ \frac{\partial Q_\theta}{r\partial\theta}+\frac{Q_r}{r}+\frac{\partial Q_r}{\partial r}+N_\theta\left(\frac{1}{r}\frac{\partial w}{\partial r}+\frac{1}{r^2}\frac{\partial^2 w}{\partial\theta^2}\right)+N_r\frac{\partial^2 w}{\partial r^2}+2N_{r\theta}\left(\frac{1}{r}\frac{\partial^2 w}{\partial r\partial\theta}-\frac{1}{r^2}\frac{\partial w}{\partial\theta}\right)+q \\ +\underline{F_r\frac{\partial w}{\partial r}\frac{1}{r\Delta\theta}+\frac{F_\theta}{r\Delta r}\frac{\partial w}{\partial\theta}+\frac{F_z}{r\Delta\theta}}=0, \\ \frac{\partial M_r}{\partial r}+\frac{\partial M_{r\theta}}{r\partial\theta}+\frac{M_r-M_\theta}{r}-Q_r+\underline{\frac{T}{r\Delta\theta}}=0, \\ \frac{\partial M_\theta}{r\partial\theta}+\frac{\partial M_{r\theta}}{\partial r}+\frac{2}{r}M_{r\theta}-Q_\theta=0, \end{cases} \tag{5}$$

where F_r, F_θ, F_z and T are internal forces per unit length along the plate–stiffener junction which are explained in detail in the following sections and Δr and $\Delta\theta$ are incremental radial and circumferential coordinates. In addition, in Eq. (5) the underlined terms are the body force terms which represent the reaction of the stiffener on the plate. These terms apply, of course, only along the plate–stiffener junction; elsewhere in the sector plate domain they are set to zero. Moreover, in-plane resultant forces N_r, N_θ and $N_{r\theta}$ and out of plane resultant forces Q_r and Q_θ and also the resultant moments M_r, M_θ and M_r can be defined by integrating corresponding stresses along the thickness as

$$\begin{cases} (N_r,N_\theta,N_{r\theta})=\int_{-h/2}^{h/2}(\sigma_r,\sigma_\theta,\sigma_{r\theta})\,dz, \\ (M_r,M_\theta,M_{r\theta})=\int_{-h/2}^{h/2}(\sigma_r,\sigma_\theta,\sigma_{r\theta})z\,dz, \\ (Q_r,Q_\theta)=K_s\int_{-h/2}^{h/2}(\sigma_{rz},\sigma_{\theta z})z\,dz, \end{cases} \tag{6}$$

in which K_s is the shear correction factor and it is assumed to be 5/6. Moreover, stress–strain relationship for FG sector plates can be written as

$$\begin{cases} \sigma_r=\frac{E(z)}{(1-\upsilon^2)}\left[\varepsilon_r+\upsilon\varepsilon_\theta-\alpha\Delta T\right], \\ \sigma_\theta=\frac{E(z)}{(1-\upsilon^2)}\left[\varepsilon_\theta+\upsilon\varepsilon_r-\alpha\Delta T\right], \\ \sigma_{r\theta}=\frac{E(z)}{2(1+\upsilon)}\varepsilon_{r\theta},\quad \sigma_{rz}=\frac{E(z)}{2(1+\upsilon)}\varepsilon_{rz},\quad \sigma_{\theta z}=\frac{E(z)}{2(1+\upsilon)}\varepsilon_{\theta z}, \end{cases} \tag{7}$$

where based on FSDT displacement field (Eq. (8)) and using the nonlinear von-Karman strain–displacement relations, Eq. (9) can be achieved

$$\begin{cases} u(r,\theta,z)=u_0(r,\theta)+z\phi_r(r,\theta), \\ v(r,\theta,z)=v_0(r,\theta)+z\phi_\theta(r,\theta), \\ w(r,\theta,z)=w(r,\theta), \end{cases} \tag{8}$$

$$\begin{cases} \varepsilon_r=\varepsilon_r^0+z\kappa_r=\frac{\partial u_0}{\partial r}+\frac{1}{2}\left(\frac{\partial w}{\partial r}\right)^2+z\frac{\partial\phi_r}{\partial r}, \\ \varepsilon_\theta=\varepsilon_\theta^0+z\kappa_\theta=\frac{1}{r}\left(u_0+\frac{\partial v_0}{\partial\theta}\right)+\frac{1}{2r^2}\left(\frac{\partial w}{\partial\theta}\right)^2+\frac{z}{r}\frac{\partial\phi_\theta}{\partial\theta}+z\frac{\phi_r}{r}, \\ \varepsilon_{r\theta}=\varepsilon_{r\theta}^0+z\kappa_{r\theta}=\frac{1}{r}\left(\frac{\partial u_0}{\partial\theta}-v_0\right)+\frac{\partial v_0}{\partial r}+\frac{1}{r}\left(\frac{\partial w}{\partial r}\right)\left(\frac{\partial w}{\partial\theta}\right)+\frac{z}{r}\frac{\partial\phi_r}{\partial\theta}+z\frac{\partial\phi_\theta}{\partial r}-z\frac{\phi_\theta}{r}, \\ \varepsilon_{rz}=\varepsilon_{rz}^0=\phi_r+\frac{\partial w}{\partial r}, \\ \varepsilon_{\theta z}=\varepsilon_{\theta z}^0=\phi_\theta+\frac{1}{r}\frac{\partial w}{\partial\theta}. \end{cases} \tag{9}$$

where $(\varepsilon_r^0, \varepsilon_\theta^0, \varepsilon_{r\theta}^0, \varepsilon_{rz}^0, \varepsilon_{\theta z}^0)$ are the membrane strains, and $(\kappa_r, \kappa_\theta, \kappa_{r\theta})$ are the flexural (bending) strains, known as the curvatures. Using Eqs. (6)–(9) gives the two following constitutive relations:

$$\begin{bmatrix} N_r \\ N_\theta \\ N_{r\theta} \\ M_r \\ M_\theta \\ M_{r\theta} \end{bmatrix}=\begin{bmatrix} A_{11} & A_{12} & 0 & B_{11} & B_{12} & 0 \\ A_{12} & A_{22} & 0 & B_{12} & B_{22} & 0 \\ 0 & 0 & A_{66} & 0 & 0 & B_{66} \\ B_{11} & B_{12} & 0 & D_{11} & D_{12} & 0 \\ B_{12} & B_{22} & 0 & D_{12} & D_{22} & 0 \\ 0 & 0 & B_{66} & 0 & 0 & D_{66} \end{bmatrix}\begin{bmatrix} \varepsilon_r^0 \\ \varepsilon_\theta^0 \\ \varepsilon_{r\theta}^0 \\ \kappa_r \\ \kappa_\theta \\ \kappa_{r\theta} \end{bmatrix}-\begin{bmatrix} N_r^T \\ N_\theta^T \\ 0 \\ M_r^T \\ M_\theta^T \\ 0 \end{bmatrix}, \tag{10}$$

$$\begin{cases} Q_r=K_sA_{66}\left(\phi_r+\frac{\partial w}{\partial r}\right), \\ Q_\theta=K_sA_{66}\left(\phi_\theta+\frac{1}{r}\frac{\partial w}{\partial\theta}\right), \end{cases} \tag{11}$$

in which the integration coefficients are defined as

$$\begin{cases} (A_{11},B_{11},D_{11})=\int_{-h/2}^{h/2}\frac{E(z)}{1-\upsilon^2}(1,z,z^2)\,dz, \\ (A_{12},B_{12},D_{12})=\int_{-h/2}^{h/2}\frac{\upsilon E(z)}{1-\upsilon^2}(1,z,z^2)\,dz, \\ (A_{66},B_{66},D_{66})=\int_{-h/2}^{h/2}\frac{E(z)}{2(1+\upsilon)}(1,z,z^2)\,dz. \end{cases} \tag{12}$$

It is notable that the mentioned integrations are computed numerically by discretizing the plate along the thickness direction. Thus, the number of mesh along the thickness should be adequate for accurate computations. The membrane forces and bending moments induced by thermal load per unit edge length in Eq. (10) can be calculated as

$$\begin{cases} N_r^T=N_\theta^T=\int_{-h/2}^{h/2}\frac{E(z)}{1-\upsilon}\alpha(z)T(z)dz, \\ M_r^T=M_\theta^T=\int_{-h/2}^{h/2}\frac{E(z)}{1-\upsilon}\alpha(z)T(z)z\,dz. \end{cases} \tag{13}$$

For thermal loading problems, it is assumed that the temperature variation is only along the thickness direction. The one-dimensional heat transfer equation for the z-direction is given by

$$-\frac{d}{dz}\left(K(Z)\frac{dT(z)}{dz}\right)=0, \tag{14}$$

hence, the temperature function $T(z)$ can be obtained easily from Eq. (14) as follows:

$$T(z)=T_m+(T_c-T_m)\int_{-h/2}^{z}\frac{dz}{K(z)}\Big/\int_{-h/2}^{h/2}\frac{dz}{K(z)}, \tag{15}$$

where $T=T_c$ at $z=h/2$ and $T=T_m$ at $z=-h/2$. It has to be noted that $T(z)$ is measured from the stress free state$T_0=0^o$ C. Substituting resultant forces and moments obtained in Eqs. (10) and (11)into Eq. (5), the five equilibrium equations are achieved in displacement field of sector plate and the reaction forces of the stiffener on the plate as

$$\begin{cases} A_{11}\left(\frac{\partial^2 u_0}{\partial r^2}+\frac{\partial^2 w}{\partial r^2}\frac{\partial w}{\partial r}+\upsilon\left(\frac{1}{r}\frac{\partial u_0}{\partial r}-\frac{u_0}{r^2}+\frac{1}{r}\frac{\partial^2 v_0}{\partial r\partial\theta}-\frac{1}{r^2}\frac{\partial v_0}{\partial\theta}-\frac{1}{r^3}\left(\frac{\partial w}{\partial\theta}\right)^2+\frac{1}{r^2}\frac{\partial^2 w}{\partial r\partial\theta}\frac{\partial w}{\partial\theta}\right)\right)\\ +B_{11}\left(\frac{\partial^2\phi_r}{\partial r^2}-\frac{\upsilon}{r^2}\frac{\partial\phi_\theta}{\partial\theta}+\frac{\upsilon}{r}\frac{\partial^2\phi_\theta}{\partial r\partial\theta}-\frac{\upsilon\phi_r}{r^2}+\frac{\upsilon}{r}\frac{\partial\phi_r}{\partial r}\right)\\ +\frac{A_{11}}{r}\left(\left(\frac{\partial u_0}{\partial r}+\frac{1}{2}\left(\frac{\partial w}{\partial r}\right)^2-\frac{u_0}{r}-\frac{1}{r}\frac{\partial v_0}{\partial\theta}-\frac{1}{2}\left(\frac{1}{r}\frac{\partial w}{\partial\theta}\right)^2\right)+\upsilon\left(\frac{u_0}{r}+\frac{1}{r}\frac{\partial v_0}{\partial\theta}+\frac{1}{2r^2}\left(\frac{\partial w}{\partial\theta}\right)^2-\frac{\partial u_0}{\partial r}-\frac{1}{2}\left(\frac{\partial w}{\partial r}\right)^2\right)\right)\\ +\frac{B_{11}}{r}\left(\frac{\partial\phi_r}{\partial r}+\frac{\upsilon}{r}\frac{\partial\phi_\theta}{\partial\theta}+\frac{\upsilon\phi_r}{r}-\frac{1}{r}\frac{\partial\phi_\theta}{\partial\theta}+\frac{\phi_r}{r}+\upsilon\frac{\partial\phi_r}{\partial r}\right)\\ +\frac{A_{66}}{r}\left(\frac{1}{r}\left(\frac{\partial^2 u_0}{\partial\theta^2}-\frac{\partial v_0}{\partial\theta}\right)+\frac{\partial^2 v_0}{\partial r\partial\theta}+\frac{1}{r}\frac{\partial^2 w}{\partial r\partial\theta}\frac{\partial w}{\partial\theta}+\frac{1}{r}\frac{\partial w}{\partial r}\frac{\partial^2 w}{\partial\theta^2}\right)+\frac{B_{66}}{r}\left(\frac{1}{r}\frac{\partial^2\phi_r}{\partial\theta^2}+\frac{\partial^2\phi_\theta}{\partial r\partial\theta}-\frac{1}{r}\frac{\partial\phi_\theta}{\partial\theta}\right)+\underline{\frac{F_r}{r\Delta\theta}}=0, \end{cases} \tag{16}$$

$$\begin{cases} A_{66}\left(-\frac{1}{r^2}\frac{\partial u_0}{\partial\theta}+\frac{1}{r}\frac{\partial^2 u_0}{\partial r\partial\theta}-\frac{1}{r}\frac{\partial v_0}{\partial r}+\frac{v_0}{r^2}+\frac{\partial^2 v_0}{\partial r^2}-\frac{1}{r^2}\frac{\partial w}{\partial r}\frac{\partial w}{\partial\theta}+\frac{1}{r}\frac{\partial^2 w}{\partial r^2}\frac{\partial w}{\partial\theta}+\frac{1}{r}\frac{\partial w}{\partial r}\frac{\partial^2 w}{\partial r\partial\theta}\right)\\ +B_{66}\left(-\frac{1}{r^2}\frac{\partial\phi_r}{\partial\theta}+\frac{1}{r}\frac{\partial^2\phi_r}{\partial r\partial\theta}+\frac{\partial^2\phi_\theta}{\partial r^2}+\frac{\phi_\theta}{r^2}-\frac{1}{r}\frac{\partial\phi_\theta}{\partial r}\right)+\\ +\frac{A_{11}}{r}\left(\frac{1}{r}\frac{\partial u_0}{\partial\theta}+\frac{1}{r}\frac{\partial^2 v_0}{\partial\theta^2}+\frac{1}{r^2}\frac{\partial^2 w}{\partial\theta^2}\frac{\partial w}{\partial\theta}+\upsilon\frac{\partial^2 u_0}{\partial r\partial\theta}+\upsilon\frac{\partial^2 w}{\partial r\partial\theta}\frac{\partial w}{\partial r}\right)+\frac{B_{11}}{r}\left(\frac{1}{r}\frac{\partial^2\phi_\theta}{\partial\theta^2}+\frac{1}{r}\frac{\partial\phi_r}{\partial\theta}+\upsilon\frac{\partial^2\phi_r}{\partial r\partial\theta}\right)\\ +\frac{2A_{66}}{r}\left(\frac{1}{r}\left(\frac{\partial u_0}{\partial\theta}-v_0\right)+\frac{\partial v_0}{\partial r}+\frac{1}{r}\frac{\partial w}{\partial r}\frac{\partial w}{\partial\theta}\right)+\frac{2B_{66}}{r}\left(\frac{1}{r}\frac{\partial\phi_r}{\partial\theta}+\frac{\partial\phi_\theta}{\partial r}-\frac{\phi_\theta}{r}\right)+\underline{\frac{F_\theta}{\Delta r}}=0, \end{cases} \tag{17}$$

$$\begin{cases} \frac{K_sA_{66}}{r}\left(\frac{\partial\phi_\theta}{\partial\theta}+\frac{1}{r}\frac{\partial^2 w}{\partial\theta^2}\right)+\frac{K_sA_{66}}{r}\left(\phi_r+\frac{\partial w}{\partial r}\right)+K_sA_{66}\left(\frac{\partial\phi_r}{\partial r}+\frac{\partial^2 w}{\partial r^2}\right)+A_{11}\left(\frac{\partial u_0}{\partial r}+\frac{1}{2}\left(\frac{\partial w}{\partial r}\right)^2+\upsilon\left(\frac{u_0}{r}+\frac{1}{r}\frac{\partial v_0}{\partial\theta}+\frac{1}{2r^2}\left(\frac{\partial w}{\partial\theta}\right)^2\right)\right)\\ \frac{\partial^2 w}{\partial r^2}+B_{11}\left(\frac{\partial\phi_r}{\partial r}+\frac{\upsilon}{r}\frac{\partial\phi_\theta}{\partial\theta}+\frac{\upsilon\phi_r}{r}\right)\frac{\partial^2 w}{\partial r^2}+A_{11}\left(\frac{u_0}{r}+\frac{1}{r}\frac{\partial v_0}{\partial\theta}+\frac{1}{2r^2}\left(\frac{\partial w}{\partial\theta}\right)^2+\upsilon\left(\frac{\partial u_0}{\partial r}+\frac{1}{2}\left(\frac{\partial w}{\partial r}\right)^2\right)\right)\frac{1}{r}\frac{\partial w}{\partial r}\\ +B_{11}\left(\frac{1}{r}\frac{\partial\phi_\theta}{\partial\theta}+\frac{\phi_r}{r}+\upsilon\frac{\partial\phi_r}{\partial r}\right)\frac{1}{r}\frac{\partial w}{\partial r}+A_{11}\left(\frac{u_0}{r}+\frac{1}{r}\frac{\partial v_0}{\partial\theta}+\frac{1}{2r^2}\left(\frac{\partial w}{\partial\theta}\right)^2+\upsilon\left(\frac{\partial u_0}{\partial r}+\frac{1}{2}\left(\frac{\partial w}{\partial r}\right)^2\right)\right)\frac{1}{r^2}\frac{\partial^2 w}{\partial\theta^2}\\ +B_{11}\left(\frac{1}{r}\frac{\partial\phi_\theta}{\partial\theta}+\frac{\phi_r}{r}+\upsilon\frac{\partial\phi_r}{\partial r}\right)\frac{1}{r^2}\frac{\partial^2 w}{\partial\theta^2}+2A_{66}\left(\frac{1}{r}\left(\frac{\partial u_0}{\partial\theta}-v_0\right)+\frac{\partial v_0}{\partial r}+\frac{1}{r}\left(\frac{\partial w}{\partial r}\right)\left(\frac{\partial w}{\partial\theta}\right)\right)\frac{1}{r}\frac{\partial^2 w}{\partial r\partial\theta}\\ +2B_{66}\left(\frac{1}{r}\frac{\partial\phi_r}{\partial\theta}+\frac{\partial\phi_\theta}{\partial r}-\frac{\phi_\theta}{r}\right)\frac{1}{r}\frac{\partial^2 w}{\partial r\partial\theta}-2A_{66}\left(\frac{1}{r}\left(\frac{\partial u_0}{\partial\theta}-v_0\right)+\frac{\partial v_0}{\partial r}+\frac{1}{r}\left(\frac{\partial w}{\partial r}\right)\left(\frac{\partial w}{\partial\theta}\right)\right)\frac{1}{r^2}\frac{\partial w}{\partial\theta}\\ -2B_{66}\left(\frac{1}{r}\frac{\partial\phi_r}{\partial\theta}+\frac{\partial\phi_\theta}{\partial r}-\frac{\phi_\theta}{r}\right)\frac{1}{r^2}\frac{\partial w}{\partial\theta}-N_\theta^T\left(\frac{1}{r}\frac{\partial w}{\partial r}+\frac{1}{r^2}\frac{\partial^2 w}{\partial\theta^2}\right)-N_r^T\frac{\partial^2 w}{\partial r^2}+q+\underline{F_r\frac{\partial w}{\partial r}\frac{1}{r\Delta\theta}+\frac{F_\theta}{r\Delta r}\frac{\partial w}{\partial\theta}+\frac{F_z}{r\Delta\theta}}=0, \end{cases} \tag{18}$$

$$\begin{cases} B_{11}\left(\frac{\partial^2 u}{\partial r^2}+\frac{\partial^2 w}{\partial r^2}\frac{\partial w}{\partial r}+\upsilon\left(-\frac{u}{r^2}+\frac{1}{r}\frac{\partial u}{\partial r}-\frac{1}{r^2}\frac{\partial v}{\partial\theta}+\frac{1}{r}\frac{\partial^2 v}{\partial r\partial\theta}-\frac{1}{r^3}\left(\frac{\partial w}{\partial\theta}\right)^2+\frac{1}{r^2}\frac{\partial^2 w}{\partial r\partial\theta}\frac{\partial w}{\partial\theta}\right)\right)+\\ D_{11}\left(\frac{\partial^2\phi_r}{\partial r^2}+\upsilon\left(-\frac{1}{r^2}\frac{\partial\phi_\theta}{\partial\theta}+\frac{1}{r}\frac{\partial^2\phi_\theta}{\partial r\partial\theta}-\frac{\phi_r}{r^2}+\frac{1}{r}\frac{\partial\phi_r}{\partial r}\right)\right)\\ +\frac{B_{66}}{r}\left(\frac{1}{r}\frac{\partial^2 u}{\partial\theta^2}+\frac{\partial^2 v}{\partial r\partial\theta}-\frac{1}{r}\frac{\partial v}{\partial\theta}+\frac{1}{r}\frac{\partial^2 w}{\partial r\partial\theta}\frac{\partial w}{\partial\theta}+\frac{1}{r}\frac{\partial w}{\partial r}\frac{\partial^2 w}{\partial\theta^2}\right)+\frac{D_{66}}{r}\left(\frac{1}{r}\frac{\partial^2\phi_r}{\partial\theta^2}+\frac{\partial^2\phi_\theta}{\partial r\partial\theta}-\frac{1}{r}\frac{\partial\phi_\theta}{\partial\theta}\right)\\ +\frac{B_{11}}{r}\left(\frac{\partial u}{\partial r}+\frac{1}{2}\left(\frac{\partial w}{\partial r}\right)^2+\upsilon\left(\frac{u}{r}+\frac{1}{r}\frac{\partial v}{\partial\theta}+\frac{1}{2r^2}\left(\frac{\partial w}{\partial\theta}\right)^2\right)\right)+\frac{D_{11}}{r}\left(\frac{\partial\phi_r}{\partial r}+\frac{\upsilon}{r}\frac{\partial\phi_\theta}{\partial\theta}+\frac{\upsilon\phi_r}{r}\right)\\ -\frac{B_{11}}{r}\left(\frac{u}{r}+\frac{1}{r}\frac{\partial v}{\partial\theta}+\frac{1}{2r^2}\left(\frac{\partial w}{\partial\theta}\right)^2+\upsilon\left(\frac{\partial u}{\partial r}+\frac{1}{2}\left(\frac{\partial w}{\partial r}\right)^2\right)\right)-\frac{D_{11}}{r}\left(\frac{1}{r}\frac{\partial\phi_\theta}{\partial\theta}+\frac{\phi_r}{r}+\upsilon\frac{\partial\phi_r}{\partial r}\right)\\ -K_sA_{66}\left(\phi_r+\frac{\partial w}{\partial r}\right)+\underline{\frac{T}{r\Delta\theta}}=0, \end{cases} \tag{19}$$

$$\begin{cases} \frac{B_{11}}{r}\left(\frac{\partial u}{r\partial\theta}+\frac{1}{r}\frac{\partial^2 v}{\partial\theta^2}+\frac{1}{r^2}\frac{\partial^2 w}{\partial\theta^2}\frac{\partial w}{\partial\theta}+\upsilon\left(\frac{\partial^2 u}{\partial r\partial\theta}+\frac{\partial^2 w}{\partial r\partial\theta}\frac{\partial w}{\partial r}\right)\right)+\frac{D_{11}}{r}\left(\frac{1}{r}\frac{\partial^2\phi_\theta}{\partial\theta^2}+\frac{1}{r}\frac{\partial\phi_r}{\partial\theta}+\upsilon\frac{\partial^2\phi_r}{\partial r\partial\theta}\right)\\ +B_{66}\left(-\frac{1}{r^2}\frac{\partial u}{\partial\theta}+\frac{1}{r}\frac{\partial^2 u}{\partial r\partial\theta}+\frac{\partial^2 v}{\partial r^2}+\frac{v}{r^2}-\frac{1}{r}\frac{\partial v}{\partial r}-\frac{1}{r^2}\frac{\partial w}{\partial r}\frac{\partial w}{\partial\theta}+\frac{1}{r}\frac{\partial^2 w}{\partial r^2}\frac{\partial w}{\partial\theta}+\frac{1}{r}\frac{\partial w}{\partial r}\frac{\partial^2 w}{\partial r\partial\theta}\right)\\ +D_{66}\left(-\frac{1}{r^2}\frac{\partial\phi_r}{\partial\theta}+\frac{1}{r}\frac{\partial^2\phi_r}{\partial r\partial\theta}+\frac{\partial^2\phi_\theta}{\partial r^2}+\frac{\phi_\theta}{r^2}-\frac{1}{r}\frac{\partial\phi_\theta}{\partial r}\right)\\ +\frac{2B_{66}}{r}\left(\frac{1}{r}\left(\frac{\partial u}{\partial\theta}-v\right)+\frac{\partial v}{\partial r}+\frac{1}{r}\left(\frac{\partial w}{\partial r}\right)\left(\frac{\partial w}{\partial\theta}\right)\right)+\frac{2D_{66}}{r}\left(\frac{1}{r}\frac{\partial\phi_r}{\partial\theta}+\frac{\partial\phi_\theta}{\partial r}-\frac{\phi_\theta}{r}\right)-K_sA_{66}\left(\phi_\theta+\frac{1}{r}\frac{\partial w}{\partial\theta}\right)=0. \end{cases} \tag{20}$$

To complete the formulation of the problem, the governing equations must be accompanied by a set of boundary conditions. The boundary conditions considered are all-round clamped and simply supported in-plane fixed. The force and displacement constraints imposed in each case are given below

(a) On the radial edges ($\theta=0^o$and $\theta=\alpha$)

for simply supported edges:

$$u=v=w=\varphi_r=M_\theta=0, \tag{21}$$

for clamped edges:

$$u=v=w=\varphi_r=\varphi_\theta=0, \tag{22}$$

(b) On the circumferential edges ($r=r_i$ and $r=r_o$)

for simply supported edges:

$$u=v=w=\varphi_\theta=M_r=0, \tag{23}$$

for clamped edges:

$$u=v=w=\varphi_r=\varphi_\theta=0, \tag{24}$$

3.2. Stiffener equations

The stiffener equilibrium equations relate the plate body forces (F_r, F_θ and F_z) and the torsional interaction couple, T to the stiffener centroidal forces and moments N_A, M_V, M_H and M_T associated with mutually perpendicular axes passing through the center of area axis of the stiffener cross-section and also the centroidal displacements, v_c and w_c, as follows [1]:

$$\begin{cases} F_r=\frac{\partial N_A}{\partial r},\\ F_\theta=-\frac{\partial^2 M_H}{\partial r^2}+\frac{\partial N_A}{\partial r}\frac{\partial v_c}{\partial r}+N_A\frac{\partial^2 v_c}{\partial r^2},\\ F_z=\frac{\partial^2 M_V}{\partial r^2}+\frac{1}{r}\frac{\partial^2 M_H}{\partial r^2}\frac{\partial w_c}{\partial\theta}+\frac{\partial^2 N_A}{\partial r^2}e+N_A\frac{\partial^2 w_c}{\partial r^2},\\ T=\frac{\partial^2 M_H}{\partial r^2}e+\frac{\partial M_T}{\partial r}. \end{cases} \tag{25}$$

In Eq. (25) M_H and M_V are the internal moments acting about vertical and horizontal axes, respectively, through the center of area of the stiffener cross-section, N_A is the force directed normal to the stiffener cross-section along the center of area axis, $e=[h^s+h_0]/2$ is the vertical distance of the center of area of the stiffener from the plate mid-plane and v_c, w_c are the displacements of the center of area in the circumferential and normal directions, respectively. Moreover, M_T is the internal torsional moment on the stiffener cross-section. It should also be appreciated that the forces per unit length, F_r, F_θ and F_z act at the level of the plate mid-plane and *not* at the top of the stiffener, which coincides with the lower surface of the plate.

The stiffener is elastic and isotropic, so that the axial force is related to the radial strain and the moments and torque are related to the curvatures and twist as follows [3]:

$$\begin{cases} N_A=(E^sh^sb^s)\varepsilon_r^{0,s},\\ M_V=\left(\frac{E^s(h^s)^3b^s}{12}\right)k_r^{0,s},\\ M_H=\left(\frac{E^sh^s(b^s)^3}{12}\right)k_\theta^{0,s},\\ M_T=\left(K^sG^sh^s(b^s)^3\right)k_{r\theta}^{0,s}, \end{cases} \tag{26}$$

where E_s and G^s are the Young and shear module of the stiffener, respectively, and K^s is a numerical factor which depends on the ratio, h^s/b^s. It should, however, be appreciated that in the parameter studies reported in the later sections of the paper twisting of the stiffener does not arise (for reasons of symmetry) [3]. Therefore, M_T is zero thus K^s and $k_{r\theta}^{0,s}$ do not need to be specified. Moreover, the relationship between the stiffener axial strain and curvatures, $\varepsilon_r^{0,s}$, $k_r^{0,s}$ and $k_\theta^{0,s}$, of Eq. (26) with the stiffener centroidal displacement components,u_c, v_c,w_c are [1]:

$$\begin{cases} \varepsilon_r^{0,s} = \frac{\partial u_c}{\partial r} + \frac{1}{2}\left(\frac{\partial w_c}{\partial r}\right)^2 + \frac{1}{2}\left(\frac{\partial v_c}{\partial r}\right)^2, \\ k_r^{0,s} = -\frac{\partial^2 w_c}{\partial r^2}, \\ k_\theta^{0,s} = -\frac{\partial^2 v_c}{\partial r^2}. \end{cases} \tag{27}$$

Two types of stiffener boundary conditions arise at the circumferential edge of the plate, i.e. at $r=r_i$, $\theta=\alpha/2$ and $r=r_o$, $\theta=\alpha/2$. At this edge, similar to those mentioned for the plate, both simply supported and clamped in-plane fixed conditions are considered. These conditions imply the following constraints on displacements and stress couples:

For simply supported edges:

$$v_c = w_c = M_V = 0, \quad u_c = -e\frac{\partial w_c}{\partial r}, \tag{28}$$

For clamped edges:

$$u_c = v_c = w_c = \frac{\partial w_c}{\partial r} = 0. \tag{29}$$

Along the plate–stiffener junction displacement continuity dictates that a relationship exists between the plate mid-plane displacements and the displacements of the center of area of the stiffener cross-section. By assuming that the stiffener eccentricity is small in relation to the plate curvature, it is reasonable to assume that the stiffener curvature is approximately equal to the plate curvature. In addition, it is assumed that the normal strains in the stiffener are negligible [3]. These simplifying assumptions allow introducing the following relationships between the displacements of the center of area of the stiffener cross-section in terms of the plate mid-plane displacements at the plate–stiffener junction

$$\begin{cases} u_c = u_0 + e\phi_r, \\ v_c = v_0 + e\phi_\theta, \\ w_c = w_0. \end{cases} \tag{30}$$

It has to be mentioned that unlike the previous studies related to the large deflection analysis of stiffened isotropic sector plate based on CPT [1–4], in this paper the large deflection analysis of stiffened FG sector plate is carried out based on FSDT. Therefore, because of the existing five plate equilibrium equations, the effect of the torsional interaction couple, T, appears explicitly in the forth plate equilibrium equations (see Eq. (5)). Hence, unlike the CPT, there is no need to use an equal and opposite pressure distributions along the length of the stiffener to provide an equivalent couple based on FSDT.

4. Solution of the stiffened FG sector plate equations

The governing stiffened FG annular sector plate equations are too complicated and are not amenable to closed-form solution. Instead, recourse must be made to a numerical solution procedure. Between the several numerical solution methods, the DR solution algorithm along with the finite difference discretization method has been adopted for the solution of the stiffened FG sector plate equations primarily because the authors have long-standing experience with this particular equation solution technique [28–32]. Here only a brief outline is presented because the equations are lengthy when presented in full. The DR method is essentially a pseudo-time-stepping initial-value technique. Therefore, to apply the DR method, it is necessary to convert the system of governing equations from boundary-value to initial-value format. This is achieved by adding damping and inertia terms to the right hand sides of Eq. (5) so that

$$LHS\ \{\text{Eq. (5)}\} = m_\lambda \frac{\partial^2 \lambda}{\partial^2 t} + c_\lambda \frac{\partial \lambda}{\partial t}. \tag{31}$$

In Eq. (31) LHS=left-hand side and m_λ, c_λ (λ:u, v, w, φ_r, φ_θ) are elements of diagonal fictitious mass and damping matrices M and C, respectively. The stability and convergence of the DR iterative procedure depend on the correct estimation of the mass matrix and nodal damping factor. According to Gershgörin theorem, the following inequality must be satisfied for determining m_{ii}^l [l:u, v, w, φ_r, φ_θ]:

$$m_{ii}^l \geq 0.25(\tau^n)^2 \sum_{j=1}^{N} \left|k_{ij}^l\right|, \tag{32}$$

where the superscript n represents the n^{th} iteration step and τ is an increment of fictitious time. The element, k_{ij}, of the stiffness matrix, K, is calculated by

$$K = \frac{\partial P}{\partial X}, \tag{33}$$

where $X = u, v, w, \varphi_r, \varphi_\theta$ is the approximate solution vector and P is the left-hand-side of the equilibrium Eq. (5). The instant critical damping factor c_i^n for node i at the n^{th} iteration is given by Zhang et al. [33] as

$$c_i^n = 2\left\{\frac{(X_i^n)^T P_i^n}{(X_i^n)^T m_{ii}^n X_i^n}\right\}^{1/2}. \tag{34}$$

To complete the transformation process, the velocity and acceleration terms are replaced with the following equivalent central finite-difference expressions:

$$\dot{X}^{n-(1/2)} = (X^n - X^{n-1})/\tau^n, \tag{35}$$

$$\ddot{X}^n = (\dot{X}^{n+(1/2)} - \dot{X}^{n-(1/2)})/\tau^n. \tag{36}$$

By substituting Eqs. (35) and (36) into the right-hand side of Eq. (31), the equilibrium equations can be rearranged into an

Table 1
Comparison the $\overline{w}$ of a CCCC stiffened annular sector plate under various transverse loading and plate thickness at ($r=(r_i+r_o)/2$, $\theta=30^\circ$) between the present solution and Ref. [3].

$\overline{q}$	$\lambda=0.02$		$\lambda=0.04$	
	$\overline{w}$ from Ref. [3]	$\overline{w}$ in Present solution	$\overline{w}$ from Ref. [3]	$\overline{w}$ in Present solution
100	0.11644	0.12014	0.09003	0.08475
200	0.22727	0.22262	0.17574	0.16485
300	0.33189	0.33162	0.26362	0.25411
400	0.43289	0.42621	0.34933	0.34595
500	0.51998	0.51999	0.42857	0.41572

initial value format as follows:

$$\begin{cases} u^{\bullet n+1/2}_i = \frac{2\tau^n}{2+\tau^n c^n_i}(m^n_{ii})^{-1}\left(\frac{\partial N_r}{\partial r}+\frac{1}{r}(N_r-N_\theta)+\frac{1}{r}\frac{\partial N_{r\theta}}{\partial\theta}+\underline{\frac{F_r}{r\Delta\theta}}\right)^n_i+\frac{2-\tau^n c^n_i}{2+\tau^n c^n_i}u^{\bullet n-1/2}_i, \\ v^{\bullet n+1/2}_i = \frac{2\tau^n}{2+\tau^n c^n_i}(m^n_{ii})^{-1}\left(\frac{\partial N_{r\theta}}{\partial r}+\frac{1}{r}\frac{\partial N_\theta}{\partial\theta}+\frac{2}{r}N_{r\theta}+\underline{\frac{F_\theta}{\Delta r}}\right)^n_i+\frac{2-\tau^n c^n_i}{2+\tau^n c^n_i}v^{\bullet n-1/2}_i, \\ w^{\bullet n+1/2}_i = \frac{2\tau^n}{2+\tau^n c^n_i}(m^n_{ii})^{-1}\left(\begin{array}{l}\frac{\partial Q_\theta}{r\partial\theta}+\frac{Q_r}{r}+\frac{\partial Q_r}{\partial r}+N_\theta\left(\frac{1}{r}\frac{\partial w}{\partial r}+\frac{1}{r^2}\frac{\partial^2 w}{\partial\theta^2}\right)+N_r\frac{\partial^2 w}{\partial r^2} \\ +2N_{r\theta}\left(\frac{1}{r}\frac{\partial^2 w}{\partial r\partial\theta}-\frac{1}{r^2}\frac{\partial w}{\partial\theta}\right)+q+\underline{F_r\frac{\partial w}{\partial r}\frac{1}{r\Delta\theta}+\frac{F_\theta}{r\Delta r}\frac{\partial w}{\partial\theta}+\frac{F_z}{r\Delta\theta}}\end{array}\right)^n_i+\frac{2-\tau^n c^n_i}{2+\tau^n c^n_i}w^{\bullet n-1/2}_i, \\ \phi^{\bullet n+1/2}_{ri} = \frac{2\tau^n}{2+\tau^n c^n_i}(m^n_{ii})^{-1}\left(\frac{\partial M_r}{\partial r}+\frac{\partial M_{r\theta}}{r\partial\theta}+\frac{M_r-M_\theta}{r}-Q_r+\underline{\frac{T}{r\Delta\theta}}\right)^n_i+\frac{2-\tau^n c^n_i}{2+\tau^n c^n_i}\phi^{\bullet n-1/2}_{ri}, \\ \phi^{\bullet n+1/2}_{\theta i} = \frac{2\tau^n}{2+\tau^n c^n_i}(m^n_{ii})^{-1}\left(\frac{\partial M_\theta}{r\partial\theta}+\frac{\partial M_{r\theta}}{\partial r}+\frac{2}{r}M_{r\theta}-Q\right)^n_i+\frac{2-\tau^n c^n_i}{2+\tau^n c^n_i}\phi^{\bullet n-1/2}_{\theta i}. \end{cases} \tag{37}$$

By integrating the velocities after each time step, the displacements can be obtained as

$$u^{n+1}=u^n+\tau^{n+1}\dot{u}^{n+(1/2)}. \tag{38}$$

Similar equations should be organized to calculate the other four displacement components, v, w, ϕ_r and φ_θ. Thus, Eqs. (37), (38) and (8)–(30) constitute the complete set of equations required for the DR algorithm. It is noted that to apply the DR method for solving the obtained system of equations, they are discretized and a central finite difference technique was used to replace the derivatives.

The algorithm follows a simple sequential procedure:

1. Initialize all variables to zero and then apply the transverse load q and maximum iteration number N.
2. Specify mass and damping matrix (M and C) using Eqs. (32) and (34).
3. Compute the velocities of the damped motion using Eq. (37).
4. Compute the displacements from the velocities using Eq. (38).
5. Apply plate and stiffener displacement boundary conditions, i.e. Eqs. (21)–(24), and (28) and (29), as appropriate.
6. Compute the stiffener displacements using Eq. (30).
7. Compute the plate and stiffener strains/curvatures using Eqs. (9) and (27).
8. Compute the plate and stiffener stress resultants/couples using Eqs. (10), (11) and (26).
9. Apply plate and stiffener force boundary conditions, i.e. Eqs. (21)–(24) and (28) and (29), as appropriate.
10. Compute the interaction forces at the plate–stiffener junction using Eq. (25).
11. Check for convergence of the calculations, i.e. the velocities are acceptably small ($\leq 10^{-9}$).
12. If the convergence criteria are satisfied print out the results, otherwise, return to step 2 and repeat the sequence of calculations in order.

A more detailed explanation of the basic DR iterative algorithm in the context of simple linear and nonlinear structural and stress analysis problems may be found elsewhere [33].

5. Comparison study

To demonstrate the efficiency and accuracy of the present solution, various samples were solved for linear/nonlinear bending analysis of annular homogeneous/FG sector plate with/without stiffener subjected to different loading and boundary conditions.

Sample 1: As a first case study, the results of our analysis for a nonlinear bending problem of a homogeneous stiffened annular sector plate under uniform mechanical loading with clamped and simply supported in plane fixed boundary conditions were compared to the results of Turvey and Salehi [3]. Comparisons of the numerical results obtained in the present study with those obtained by Turvey and Salehi [3] are shown in Tables 1 and 2. The results are for dimensionless deflection $\overline{w}=w/h$ at ($\theta=30^o$, $r=(r_i+r_o)/2$) of a 60^o isotropic and homogeneous stiffened annular sector plate with inner to outer radius ratio of $\eta=r_i/r_o=0.5$, two different ratios of thickness to outer radius of $\lambda=h/r_o=0.02, 0.04$, the stiffener depth to the plate thickness of $\xi=h^s/h=1$, and subjected to different transverse loadings $\overline{q}=(qr_o^4/E_ch^4)$. The material properties of the sector plate and stiffener are identical. It is notable that because of the differences between CPT and FSDT which is applied for numerical analysis in Ref. [3] and in the present study, respectively, the obtained results are smaller than those of [3] for deflection values for both CCCC and SSSS stiffened annular sector plates with $\lambda=0.02, 0.04$. However, it is seen that there is a good agreement in Tables 1 and 2 and the validity of the present numerical method is verified.

Table 2
Comparison the $\overline{w}$ of a SSSS stiffened annular sector plate under various transverse loading and plate thickness at ($r=(r_i+r_o)/2$, $\theta=30^o$) between the present solution and Ref. [3].

$\overline{q}$	$\lambda=0.02$		$\lambda=0.04$	
	$\overline{w}$ from Ref. [3]	$\overline{w}$ in Present solution	$\overline{w}$ from Ref. [3]	$\overline{w}$ in Present solution
100	0.345454	0.35446	0.30545	0.28753
200	0.536363	0.53102	0.49091	0.42296
300	0.69901	0.69521	0.62727	0.61649
400	0.79091	0.75568	0.72727	0.71960
500	0.87272	0.83977	0.81083	0.78236

Table 3
Comparisons of deflection obtained by present work with those of Nath et al. [35] for nonlinear bending of fully clamped moderately thick isotropic annular sector plates ($\lambda=h/r_o=0.2$, $\alpha=60^\circ$) for $\overline{q}=500$ at ($\overline{r}^*=r-r_i/r_o-r_i=0.176471$, $\theta=\alpha/2=30^\circ$).

Method	$\overline{w}$		
	$\mu=0.05$	$\mu=0.1$	$\mu=0.2$
Present study	0.32581	0.41711	0.57013
Ref. [35]	0.30596	0.39811	0.56931

Sample 2: In the second example, to investigate the accuracy of the current study, the dimensionless deflection ($\overline{w}=w/h$) at the point of $\bar{r}^{*}=r-\ r_i/r_o-r_i=\ 0.176471$, $\theta=\alpha/2=30^{o}$ for fully clamped moderately thick isotropic un-stiffened sector plate ($\lambda=h/r_o=\ 0.2$, $\alpha=60^{\circ}$) subjected to uniform loading $\overline{q}\ =\ (qr_o^4/E_ch^4)=500$ with different inner to outer radius ratios $\mu=r_i/r_o$ are compared with those reported by Nath et al. [35] based on the FSDT. Good agreement is observed in Table 3 between the results of present study with those of Ref. [35].

Sample 3: In this section as a part of validation of our analysis, the present results for the linear behavior of un-stiffened annular moderately thick FG sector plates subjected to uniform transverse loading q are compared with those obtained by Ref. [15] based on FSDT. The material is made from a mixture of aluminum (metal) and zirconia (ceramic) with material properties: $E_m=70\ GPa$, $\nu_m=0.3$, $E_c=\ 151\ GPa$ and $\nu_c=0.3$. Comparisons between the results of present work and those obtained by Aghdam et al. [15] are shown in Fig. 3 for the dimensionless deflection and rotations ($\overline{W}=1000wE_ch^3/\ qr_o^4$, $\overline{\phi}_\theta=\ 100\phi_\theta E_ch^3/qr_o^3$, $\overline{\phi}_r=100\phi_rE_ch^3/qr_o^3$) along the radial and circumential directions. Again, it is clear that the present results are in good agreement with the analytical solutions obtained by Aghdam et al. [15]

As it observed, the obtained results from three above examples for the linear/nonlinear bending analysis of thin to moderately thick annular homogeneous/FG sector plates with/without stiffener showed good agreements with the results obtained by Ref. [3,35,15], and therefore, the reliability and accuracy of the present method is verified.

6. Parameter study results and discussion

In this study, the nonlinear bending of a functionally graded stiffened annular sector plate was numerically studied under combined transverse uniform and thermal gradient along thickness direction loadings. The material properties of FGM are varied through the thickness of plate according to the simple rule of mixture and are assumed as $E_m=70\,\text{GPa}$, $E_c=151\,\text{GPa}$ and $\nu_m=\nu_c=0.3$ for metal, aluminum and ceramics, zirconia, respectively (taken from [34]). The ceramic rich top surface of the FG sector plate was maintained at 300 °C,and the metal rich bottom surface was maintained at 20 °C. The stress-free temperature is $T_0=0\ ^{\circ}\text{C}$. A transverse uniform loading of $\overline{q}=500$ was also applied to the top surface of the stiffened FG plate with sector angle of $\alpha=60^{\circ}$ in which the ratio of thickness to external radius and the stiffener depth to the plate thickness are $\lambda=h/r_o=\ 0.04$ and, $\xi=h^s/h=1$, respectively. Moreover, the ratio of the inner to outer radius of annular sector plate was assumed as $\eta=r_i/r_o=0.4$. It is also noticed that the width of rectangular cross-sectional stiffener (which is oriented eccentrically at $\theta=\alpha/2=30^{\circ}$) is equal to its height and the material property of the radial stiffener is identical to the metallic phase of FG sector plate. As a result of the study, the modified mesh size of $N\times M\times K=12\times12\times20$ was selected along the radial, circumferential and thickness of the sector plate, respectively, in order to achieve the responses more accurately. The results presented in terms of the following dimensionless quantities, $\overline{w}=w/h$, $\overline{N}_r=N_rr_o^2/E_ch^3$, $\overline{M}_r=M_rr_o^2/E_ch^4$, $\overline{q}=qr_o^4/E_ch^4$, which are the dimensionless deflection, radial membrane force, radial moment and load, respectively. For a more comprehensive study, different boundary conditions, namely simply supported and clamped in plane fixed, are considered for whole edges of the sector plate and stiffener. In the following results, parametric study is carried out to investigate the effects of material grading index, boundary condition, stiffener depth to the plate thickness ratio and thermal gradient on the large deflection thermoelastic behavior of functionally graded stiffened annular sector plates. Tables 4 and 5 indicate the comparisons of maximums deflection ($\overline{w}_{\max}=w_{\max}/h$) and radial moment resultant ($\overline{M}_{r\,\max}=\ M_{r\,\max}r_o^2/E_ch^4$) obtained by linear and nonlinear analyses of CCCC and SSSS

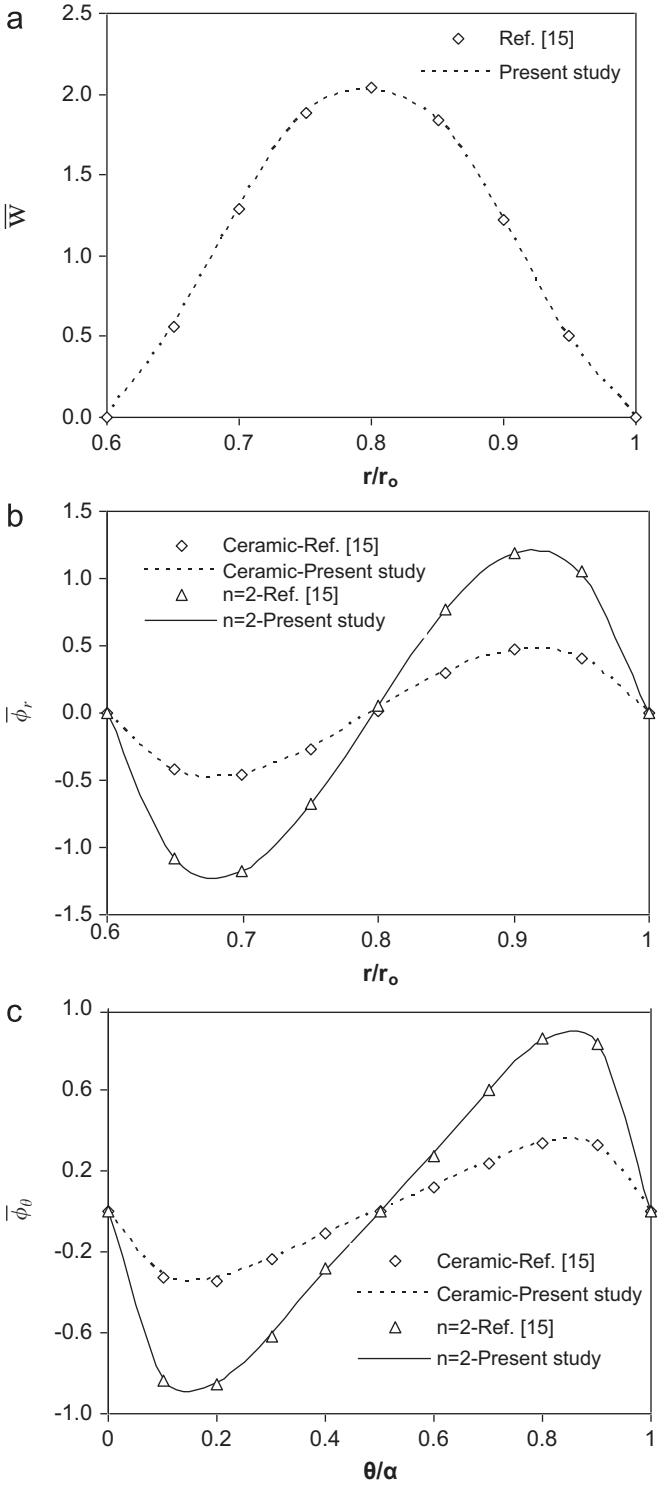

Fig. 3. Comparisons between the present study and the results obtained by Aghdam et al. [15] for the dimensionless deflection and rotations (a) $\overline{W}$, (b) $\overline{\varphi}_r$ and (c) $\overline{\varphi}_\theta$ along the radial ($\theta=\alpha/2$) and circumferential ($\overline{r}=(r_o+r_i)/2$) directions of annular moderately thick FG sector plates.

stiffened annular FG sector plates subjected to different transverse loadings with $n=0.5$, 1.0, 5.0 and ($h/r_o=0.07, 0.1$). As seen in Tables 4 and 5, unlike $\overline{M}_{r\ \max}$, with increasing of grading index n the values of $\overline{w}_{\max}$ increase for both CCCC and SSSS boundary conditions. Moreover, by increasing n the differences between $\overline{w}_{\max}$ of linear and nonlinear analyses are increased. For instance, the predicted values of $\overline{w}_{\max}$ based on linear analysis of CCCC stiffened annular FG sector plate under ($\overline{q}=500$) with $n=2.0$ and $h/r_o=0.07, 0.1$ are about 6.9% and 7.7% larger than those of nonlinear ones, respectively. It is notable that these values are about 7.5% and 10.3% for $n=5.0$, respectively. While for SSSS boundary condition with $n=2.0$ and $h/r_o=0.07, 0.1$ they are about 25.8% and 20.8%, respectively. Moreover, the mentioned values for $n=5.0$, are 24.6% and 18.5%, respectively. Therefore, unlike the CCCC boundary condition, with increasing the grading index n and thickness radius ratio h/r_o, the differences between

Table 4
Comparisons of maximums deflection ($\overline{w}_{\max}=w_{\max}/h$) and radial moment resultant ($\overline{M}_{r\ \max}=M_{r\ \max}r_o^2/E_ch^4$) obtained by linear and nonlinear analyses for CCCC stiffened annular FG sector plate subjected to different transverse loadings with $n=0.5$, 1.0, 5.0 and ($h/r_o=0.07, 0.1$).

$\overline{q}=\frac{qr_o^4}{E_mh^4}$	Grading index, n	($h/r_o=0.07$)				($h/r_o=0.1$)			
		Linear analysis		Nonlinear analysis		Linear analysis		Nonlinear analysis	
		$\overline{w}_{\max}$	$\overline{M}_{r\ \max}$	$\overline{w}_{\max}$	$\overline{M}_{r\ \max}$	$\overline{w}_{\max}$	$\overline{M}_{r\ \max}$	$\overline{w}_{\max}$	$\overline{M}_{r\ \max}$
10	0.5	0.0134	0.0265	0.0134	0.0265	0.0142	0.0236	0.0142	0.0237
	2.0	0.0163	0.0248	0.0163	0.0249	0.0168	0.0212	0.0168	0.0213
	5.0	0.0181	0.0257	0.0181	0.0257	0.0183	0.0216	0.0183	0.0217
50	0.5	0.0673	0.1328	0.0674	0.1338	0.0709	0.1186	0.0794	0.1195
	2.0	0.0818	0.1247	0.0819	0.1262	0.0839	0.1067	0.0837	0.1082
	5.0	0.0907	0.1289	0.0908	0.1303	0.0915	0.1088	0.0914	0.1100
100	0.5	0.1347	0.2663	0.1346	0.2696	0.1418	0.2383	0.1413	0.2413
	2.0	0.1637	0.2504	0.1634	0.2561	0.1674	0.2149	0.1666	0.2201
	5.0	0.1814	0.2590	0.1811	0.2639	0.1825	0.2191	0.1816	0.2231
200	0.5	0.2693	0.5348	0.2675	0.5445	0.2827	0.4799	0.2787	0.4870
	2.0	0.3269	0.5043	0.3233	0.5224	0.3329	0.4347	0.3264	0.4494
	5.0	0.3619	0.5217	0.3578	0.5356	0.3621	0.4430	0.3548	0.4526
300	0.5	0.4035	0.8047	0.3964	0.8187	0.4221	0.7238	0.4088	0.7294
	2.0	0.4890	0.7805	0.4759	0.7904	0.4956	0.6575	0.4751	0.6780
	5.0	0.5407	0.7862	0.5251	0.8051	0.5379	0.6696	0.5147	0.6780
400	0.5	0.5369	1.0752	0.5194	1.0872	0.5595	0.9686	0.5298	0.9626
	2.0	0.6494	1.0176	0.6168	1.0533	0.6551	0.8821	0.6109	0.8989
	5.0	0.7168	1.0511	0.6802	1.0651	0.7099	0.8977	0.6593	0.8925
500	0.5	0.6693	1.3456	0.6354	1.3462	0.6947	1.2134	0.6409	1.1834
	2.0	0.8075	1.2746	0.7512	1.3065	0.8117	1.1076	0.7335	1.1084
	5.0	0.8896	1.3148	0.8223	1.3114	0.8791	1.1272	0.7888	1.0929

Table 5
Comparisons of maximums deflection ($\overline{w}_{\max}=w_{\max}/h$) and radial moment resultant ($\overline{M}_{r\ \max}=M_{r\ \max}r_o^2/E_ch^4$) obtained by linear and nonlinear analyses for SSSS stiffened annular FG sector plate subjected to different transverse loadings with $n=0.5$, 2.0, 5.0 and ($h/r_o=0.07, 0.1$)

$\overline{q}=\frac{qr_o^4}{E_mh^4}$	Grading index, n	($h/r_o=0.07$)				($h/r_o=0.1$)			
		Linear analysis		Nonlinear analysis		Linear analysis		Nonlinear analysis	
		$\overline{w}_{\max}$	$\overline{M}_{r\ \max}$	$\overline{w}_{\max}$	$\overline{M}_{r\ \max}$	$\overline{w}_{\max}$	$\overline{M}_{r\ \max}$	$\overline{w}_{\max}$	$\overline{M}_{r\ \max}$
10	0.5	0.0220	0.0465	0.0219	0.0464	0.0187	0.0382	0.0168	0.0382
	2.0	0.0225	0.0444	0.0254	0.0443	0.0208	0.0347	0.0208	0.0347
	5.0	0.0275	0.0444	0.0274	0.0443	0.0219	0.0339	0.0219	0.0339
50	0.5	0.1104	0.2328	0.1079	0.2299	0.0937	0.1918	0.0926	0.1909
	2.0	0.1278	0.2226	0.1238	0.2193	0.1046	0.1746	0.1029	0.1741
	5.0	0.1376	0.2226	0.1340	0.2197	0.1102	0.1707	0.1090	0.1705
100	0.5	0.2205	0.4659	0.2100	0.4526	0.1877	0.3848	0.1823	0.3794
	2.0	0.2551	0.4460	0.2388	0.4309	0.2096	0.3511	0.2022	0.3474
	5.0	0.2746	0.4457	0.2594	0.4318	0.2212	0.3434	0.2150	0.3406
200	0.5	0.4385	0.9300	0.3944	0.8665	0.3749	0.7711	0.3487	0.7372
	2.0	0.5057	0.8903	0.4420	0.8229	0.4190	0.7055	0.3844	0.6791
	5.0	0.5436	0.8878	0.4810	0.8217	0.4422	0.6896	0.4106	0.6656
300	0.5	0.6514	1.3865	0.5535	1.2351	0.5588	1.1523	0.4947	1.0600
	2.0	0.7477	1.3248	0.6136	1.1717	0.6232	1.0544	0.5422	0.9816
	5.0	0.8015	1.3163	0.6669	1.1630	0.6571	1.0281	0.5800	0.9592
400	0.5	0.8572	1.8308	0.6910	1.5625	0.7370	1.5228	0.6213	1.3469
	2.0	0.9783	1.7434	0.7602	1.4826	0.8188	1.3908	0.6779	1.2539
	5.0	1.0452	1.7250	0.8243	1.4624	0.8615	1.3515	0.7252	1.2207
500	0.5	1.0547	2.2599	0.8114	1.8552	0.9078	1.8790	0.7318	1.6023
	2.0	1.1962	2.1431	0.8875	1.7626	1.0043	1.7114	0.7957	1.4995
	5.0	1.2735	2.1111	0.9599	1.7279	1.0445	1.5357	0.8508	1.4545

linear and nonlinear results decrease for SSSS ones. Figs. 4 and 5, respectively, illustrate vertical displacement, radial forces and moments ($\overline{w}$, $\overline{N}_r$ and $\overline{M}_r$) along radial and circumferential directions of fully clamped (CCCC) stiffened annular FG sector plate under a uniform mechanical loading ($\overline{q}=500$) and different material grading indices n. It is notable that Figs. 4 and 5 are related to $\theta=30^\circ$ and $\overline{r}=0.75$, respectively. As it is expected, more absolute values of $\overline{w}$ and$\overline{N}_r$are resulted when material grading index n increases which is caused by reduction of stiffness of plate and tendency of material property toward metallic phase. Moreover, as it is observed from Fig. 4(c), $\overline{M}_r$ has its maximum value at $\overline{r}=0.75$ for different grading indices n and when n increases, the absolute values of $\overline{M}_r$ decreases. It is noted that in Fig. 5 due to symmetry of boundary condition and loading, variations of $\overline{w}$, $\overline{N}_r$ and $\overline{M}_r$ are illustrated along the circumferential direction from $\theta=0^\circ$ to $\theta=30^\circ$. As it is observable from Fig. 5a, as θ approaches to the stiffener orientation in $\theta=30^\circ$, slope of $\overline{w}$ decreases due to increase of plate stiffness. Similar results are taken place for $\overline{N}_r$ and $\overline{M}_r$ so that increasing of θ from 0° to 15°cause increasing of $\overline{N}_r$ and $\overline{M}_r$ more sharply compared to those of θ from 15° to 30°.

Similar to Figs. 4 and 5, Figs. 6 and 7 present the variation of $\overline{w}$, $\overline{N}_r$ and $\overline{M}_r$ along the radial and circumferential directions of stiffened annular FG sector plate with simply supported in plane fixed boundary condition. The main results obtained with SSSS constraints are the same as CCCC. However, the major differences are the more absolute values of $\overline{w}$, $\overline{N}_r$ and $\overline{M}_r$ with using of SSSS

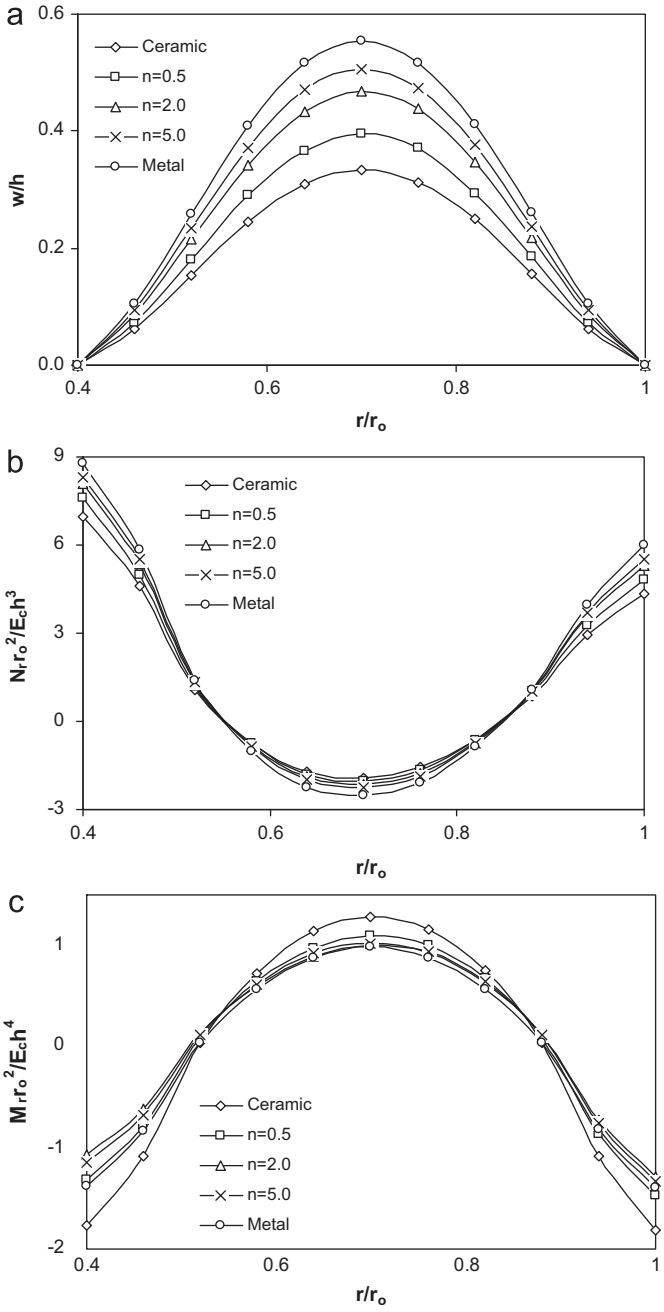

Fig. 4. (a) Vertical displacement, $\overline{w}$, (b) radial forces, $\overline{N}_r$, and (c) moments, $\overline{M}_r$, along radial direction of CCCC stiffened FG sector plate under a uniform loading ($\overline{q}=500$) with ($h/r_o=0.04$).

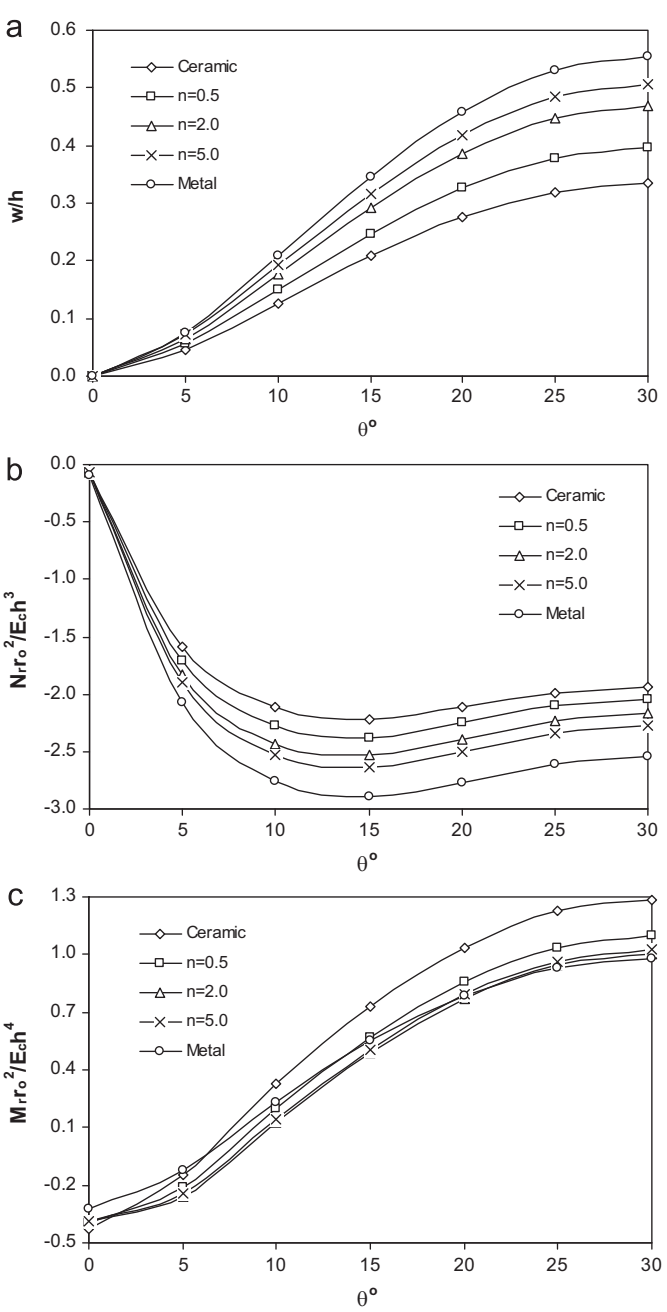

Fig. 5. (a) Vertical displacement, $\overline{w}$, (b) radial forces, $\overline{N}_r$, and (c) moments, $\overline{M}_r$, along circumferential direction of CCCC stiffened FG sector plate under a uniform loading ($\overline{q}=500$) with ($h/r_o=0.04$).

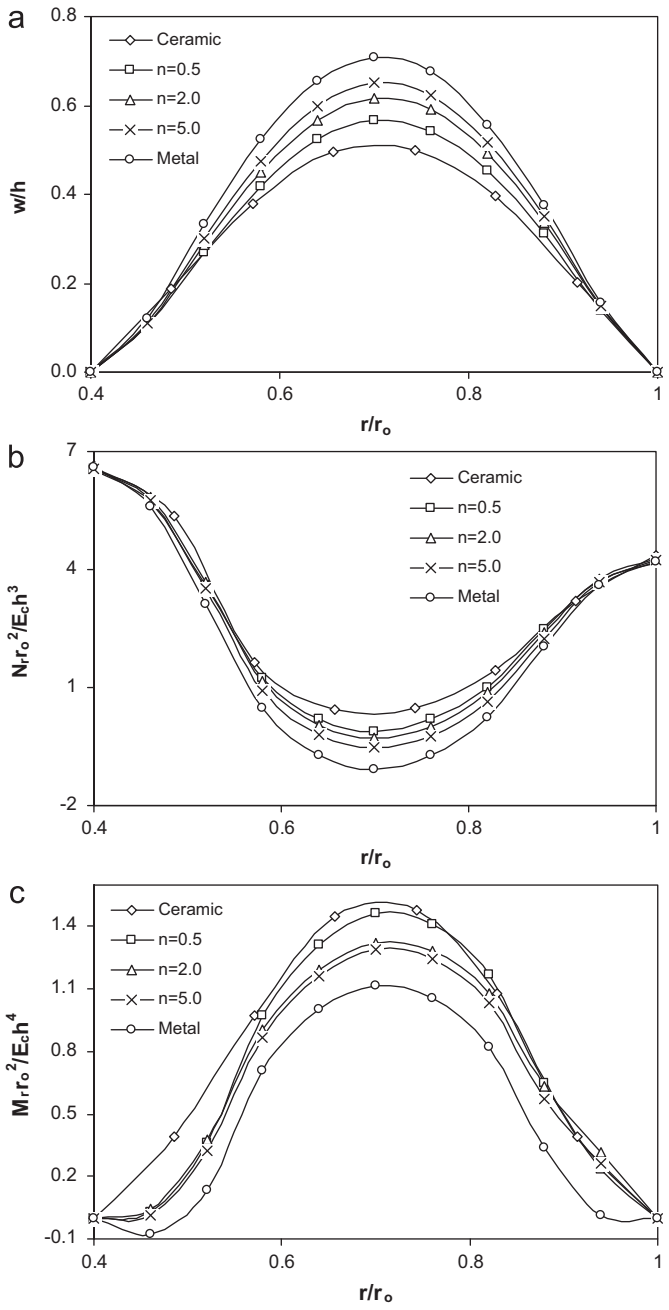

Fig. 6. (a) Vertical displacement, $\overline{w}$, (b) radial forces, $\overline{N}_r$, and (c) moments, $\overline{M}_r$, along the radial direction of SSSS stiffened FG sector plate under a uniform loading ($\overline{q}=500$) with ($h/r_o=0.04$) .

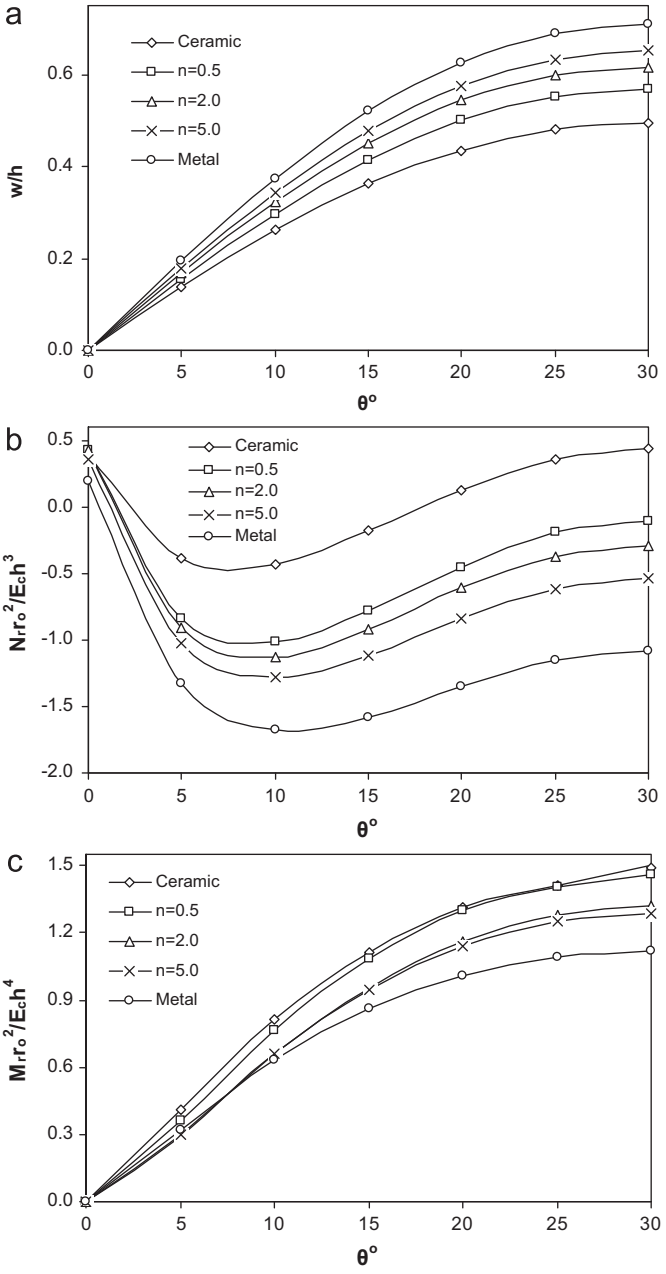

Fig. 7. (a) Vertical displacement, $\overline{w}$, (b) radial forces, $\overline{N}_r$, and (c) moments, $\overline{M}_r$, along circumferential direction of SSSS stiffened FG sector plate under a uniform loading ($\overline{q}=500$) with ($h/r_o=0.04$) .

compared to CCCC restraint and also the greater effect of grading index n and stiffener on the results. For example, the effect of stiffener on the decrease of absolute values of $\overline{N}_r$ is more noticeable in SSSS boundary condition rather than CCCC.

Figs. 8 and 9 show the effect of stiffener height on the dimensionless values of $\overline{w}$, $\overline{N}_r$ and $\overline{M}_r$ along the radial direction of a stiffened annular FG sector plate under a uniform transverse load $\overline{q}=500$ for different material grading indices n and two different boundary conditions CCCC and SSSS, respectively. The letters a and b in these figures indicate the ratio of stiffener depth to plate thickness which are taken as $\xi=1$ and $\xi=2$, respectively. As expected, by increasing the stiffener depth to plate thickness ratio, ξ, and consequently increasing the stiffness of the plate, the deflections decrease significantly, so that the difference of dimensionless deflection $\overline{w}$ between $\xi=1$ and $\xi=2$ is increased by increasing the material grading index n and tendency of material toward the homogeneous metallic phase. For instance, for $n=0.1$ and $n=10$, the maximum dimensionless deflection $\overline{w}$ for $\xi=1$ about 2.4 and 2.7 times greater than that of $\xi=2$ for clamped boundary condition (CCCC). These differences for simply supported boundary conditions (SSSS) are about 4 and 4.2 times when applying $\xi=1$ and $\xi=2$, respectively, see Figs. 8 and 9(a). At the same place, $\overline{r}=0.7$, similar trend are observed for $\overline{N}_r$ and $\overline{M}_r$, so that the values of $\overline{N}_r$ and $\overline{M}_r$ for $n=0.1$ and $n=10$ with $\xi=1$ are about 1.4 and 2.8 times greater than that of $\xi=2$, respectively, for CCCC stiffened sector plate (see Fig. 8(b) and (c)). As it is seen, these differences increase significantly when simply supported boundary conditions are used (see Fig. 9(b) and (c)).

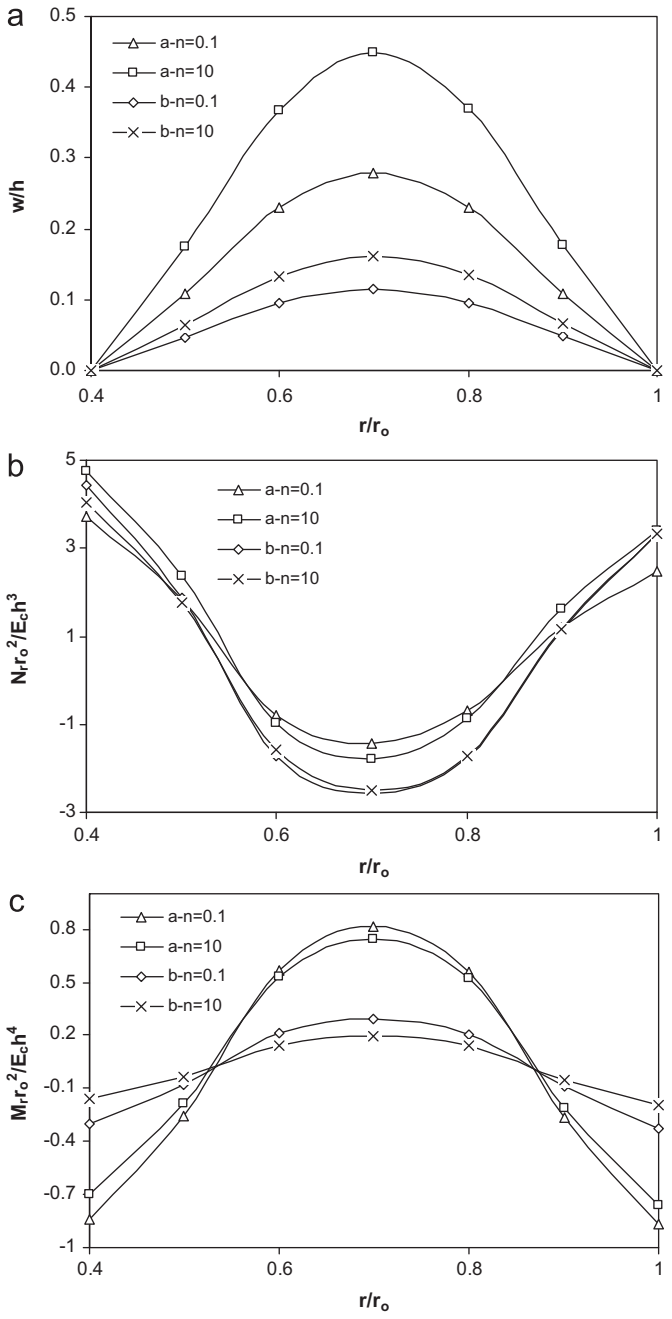

Fig. 8. Effect of stiffener height on the values of (a) $\overline{w}$, (b) $\overline{N}_r$ and (c) $\overline{M}_r$ along the radial direction of a CCCC stiffened annular FG sector plate under a uniform transverse load ($\overline{q}=500$) with ($h/r_o=0.04$) (letters *a* and *b* indicate that the ratio of stiffener depth to plate thickness are $\xi=1$ and $\xi=2$, respectively).

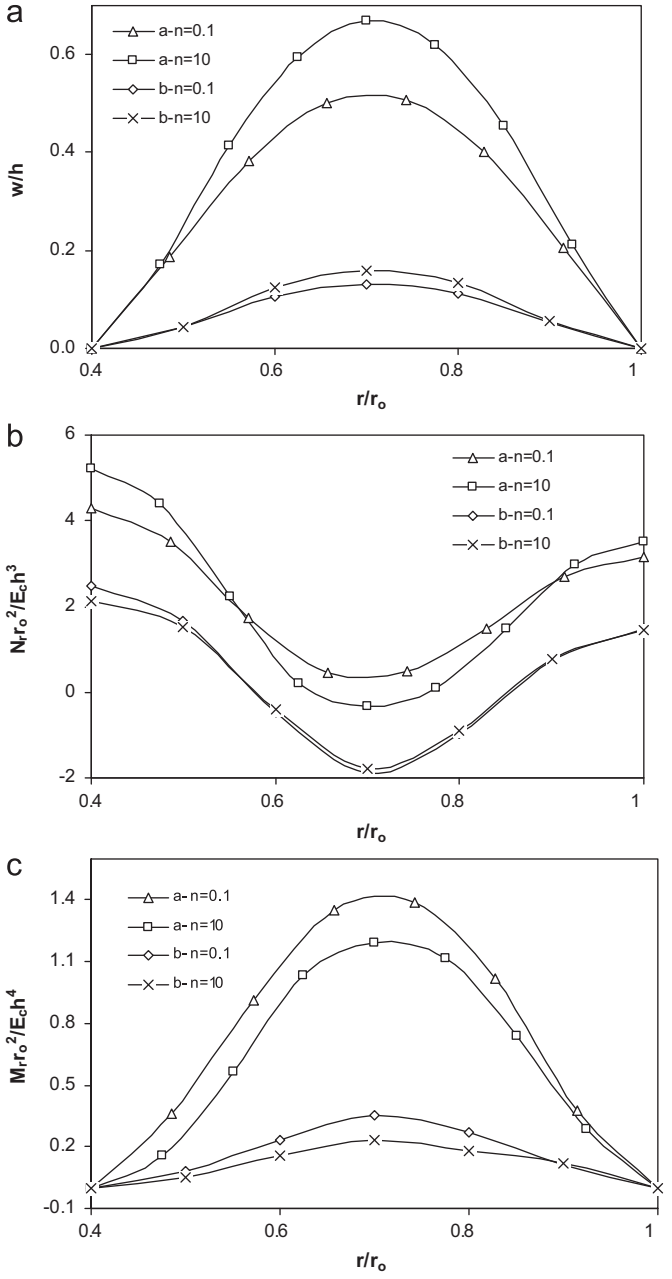

Fig. 9. Effect of stiffener height on the values of (a) $\overline{w}$, (b) $\overline{N}_r$ and (c) $\overline{M}_r$ along the radial direction of a SSSS stiffened annular FG sector plate under a uniform transverse load $\overline{q}=500$ with ($h/r_o=0.04$) (letters *a* and *b* indicate that the ratio of stiffener depth to plate thickness are $\xi=1$ and $\xi=2$, respectively).

In Fig. 10, the effect of thermal gradient on the variation of $\overline{w}$, $\overline{N}_r$ and $\overline{M}_r$ along the radial direction of a simply supported stiffened annular FG sector plate with $n=0.1$ and $n=10$ is shown. In this figure letters *a* and *b* indicate mechanical and thermo-mechanical loadings and the thermal gradient and mechanical loading are applied with $\Delta T=300$ °C and $\overline{q}=500$, respectively. It is depicted in Fig. 10 that by applying thermal gradient through the thickness of FG sector plate, the absolute values of $\overline{w}$, $\overline{N}_r$ and $\overline{M}_r$ increase which can be attributed to the additional produced thermal strains and stresses. Similar to Fig. 10, Figs. 11 and 12 illustrate the variation of $\overline{w}$, $\overline{N}_r$ and $\overline{M}_r$ along the radius of CCCC and SSSS stiffened annular FG sector plates, respectively, under mechanical and thermo-mechanical loadings with $h/r_o=0.1$ and $n=0.1$, 10. It is obvious that with increasing the material grading index from 0.1 to 10, the effect of thermal loading on the results increases due to the tendency of material toward metallic phase with higher values of thermal expansion coefficient α. Furthermore, with increasing the thickness to radius ratio the effect of thermal loading on the results decreases, see Figs. 10 and 12. However, the effect of thermal gradient on the results increases when simply supported boundary conditions are applied compared to clamped one, see Figs. 11 and 12.

7. Conclusions

Large deflection behavior of stiffened annular FG sector plates under thermo-mechanical loading and various boundary conditions was investigated. The mechanical and thermal properties of

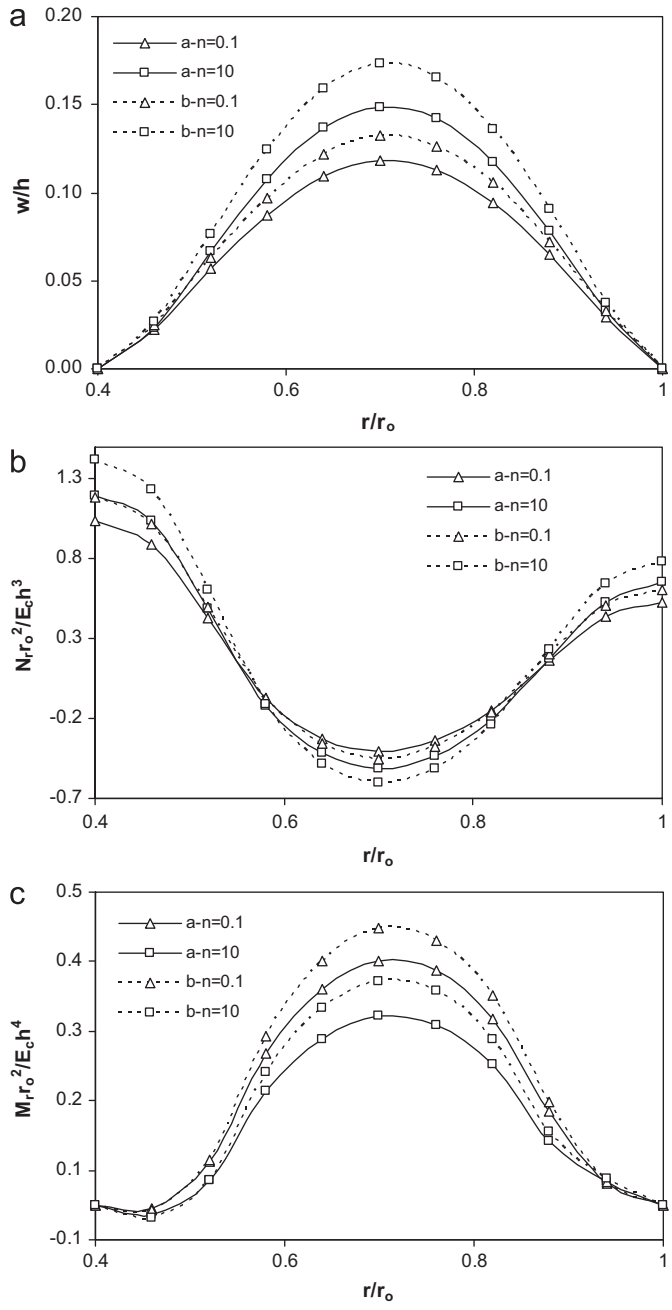

Fig. 10. Effect of thermal gradient on the variation of $\overline{w}$, $\overline{N}_r$ and $\overline{M}_r$ along radial direction of a SSSS stiffened annular FG sector plate under a uniform load $\overline{q}=500$ with $(h/r_o=0.04)$ (letters *a* and *b* specify the mechanical and thermo-mechanical loading, respectively).

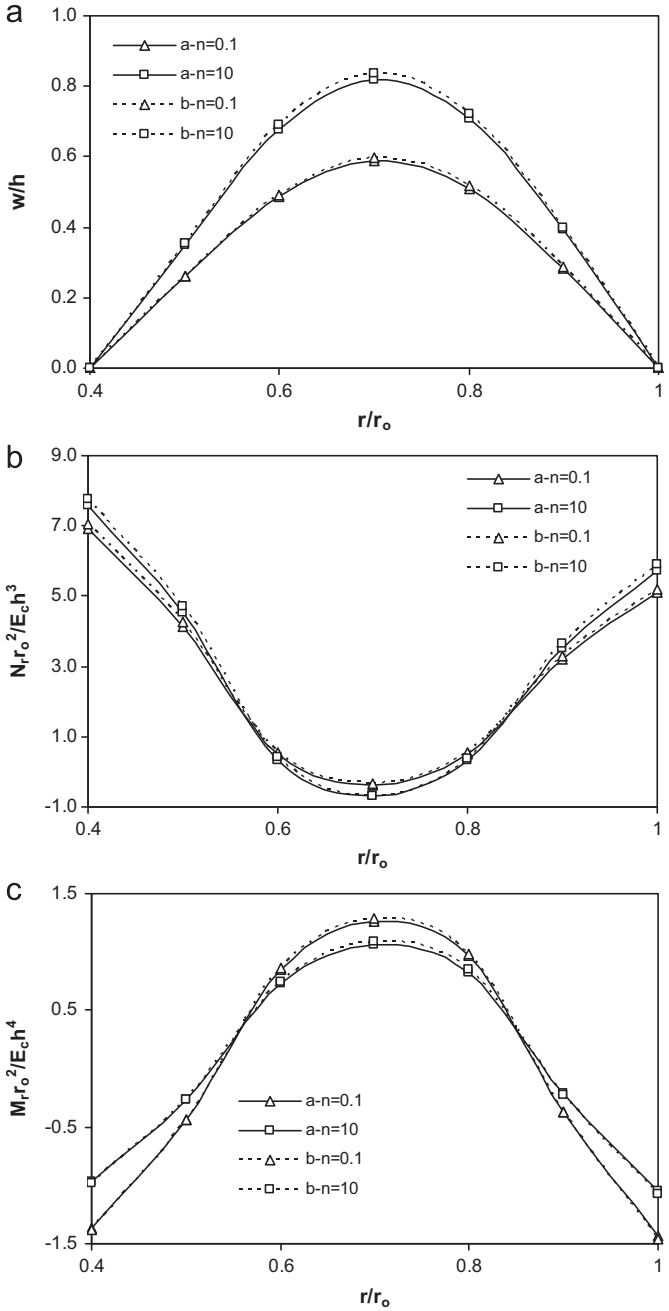

Fig. 11. The variation of $\overline{w}$, $\overline{N}_r$ and $\overline{M}_r$ along the radial direction of a CCCC stiffened annular FG sector plate under a uniform load $\overline{q}=500$ with $(h/r_o=0.1)$ (letters *a* and *b* specify the mechanical and thermo-mechanical loadings, respectively).

FGM were assumed to vary continuously throughout the thickness of plate in accordance with a simple power law of volume fraction of constituent material. Based on FSDT and using the von-Karman theory for large deflections, the nonlinear equilibrium equations were developed, and a dynamic relaxation method combined with a finite difference discretization technique was used to solve these equations. Effects of material grading index, boundary condition, the stiffener depth to the plate thickness ratio and thermal gradient were studied. Some general inferences are mentioned as below:

- When material grading index n increases, unlike $\overline{M}_r$, more absolute values of $\overline{w}$ and $\overline{N}_r$ are resulted which is caused by reduction of stiffness of plate and tendency of material property toward metallic phase.
- By increasing the stiffener depth to the plate thickness ratio, maximum values of dimensionless deflection, radial forces and moments ($\overline{w}$, $\overline{N}_r$ and $\overline{M}_r$) are decreased. Moreover, by increasing of the material grading index n and tendency of material toward the homogeneous metallic phase, the effect of stiffener is magnified.
- Effects of stiffener depth on decrease of absolute values of $\overline{w}$, $\overline{N}_r$ and $\overline{M}_r$ are more noticeable in SSSS boundary condition rather than CCCC.
- By applying thermal loading through the thickness of stiffened FG sector plate, the absolute values of $\overline{w}$, $\overline{N}_r$ and $\overline{M}_r$ are increased which can be attributed to the additional produced thermal strains and stresses.

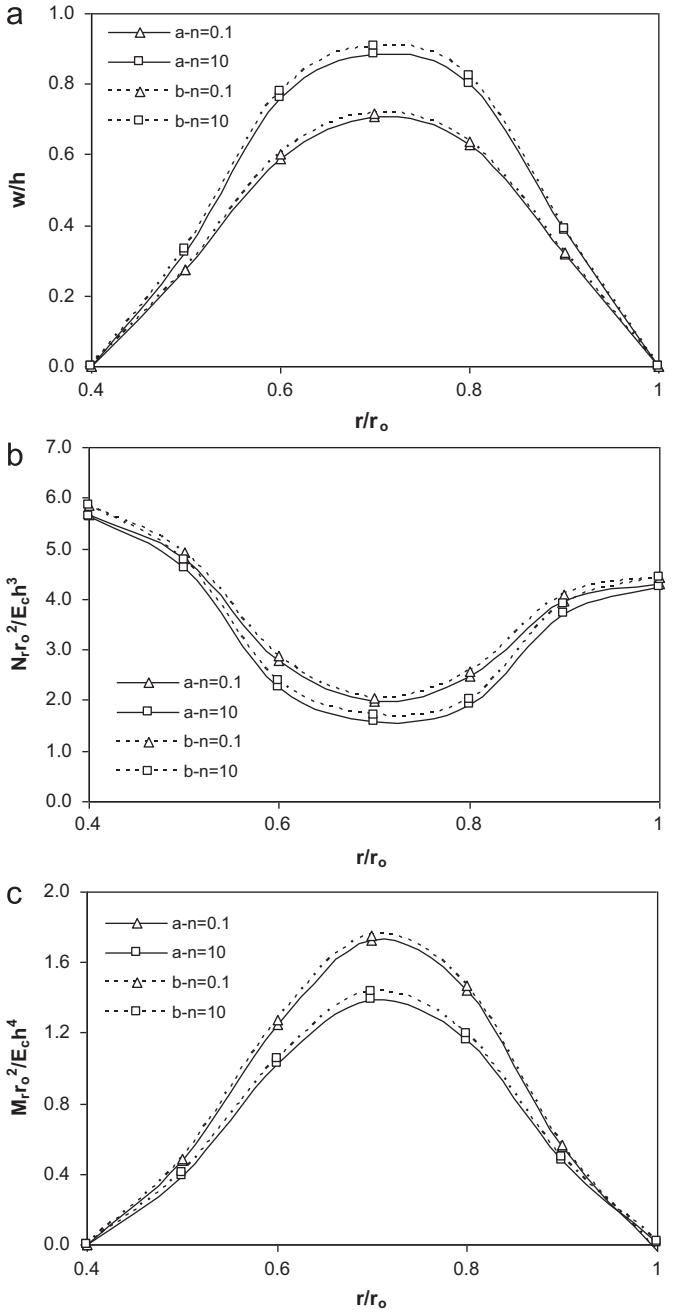

Fig. 12. The variation of $\overline{w}$, $\overline{N}_r$ and $\overline{M}_r$ along the radial direction of a SSSS stiffened annular FG sector plate under a uniform load $\overline{q}=500$ with $(h/r_o=0.1)$ (letters *a* and *b* specify the mechanical and thermo-mechanical loading, respectively).

References

[1] Turvey GJ, Salehi M. Circular plates with one diametral stiffener— an elastic large deflection. Comput Struct 1997;63(4):775–83.

[2] Turvey GJ, Der Avanessian NGV. Elastic large deflection analysis of ring-stiffened circular plates using graded finite-differences. In: Proceedings of the 1st International Conference on Numerical Methods in Engineering: Theory and Applications, University College, Swansea; 1985.

[3] Turvey GJ, Salehi M. Elastic large deflection analysis of stiffened annular sector plates. Int J Mech Sci 1998;40(1):51–70.

[4] Turvey GJ, Salehi M. Large defection analysis of eccentrically stiffened sector plates. Comput Struct 1998;68:191–205.

[5] Basu, AK, Djahani P, Dowling PJ, 1977. Elastic post-buckling behavior of discretely stiffened plates. In: Colloquium on the stability of steel structures, Liege, Belgium.

[6] Troitsky MS. Stiffened Plates, Bending, Stability and Vibrations. Amsterdam: Elsevier Scientific Publishing Company; 1976.

[7] Turvey GJ. Axisymmetric elastic large deflection behavior of stiffened composite plates. Compos Struct 2, Barking Appl Sci 1983;6:72–88.

[8] Turvey GJ, Der Avanessian NGV. Axisymmetric elasto-plastic large deflection response of ring stiffened circular plates. Int J Mech Sci 1989;31(11/12):905–24.

[9] Turvey GJ, Der Avanessian NGV. Full-range response of clamped ring-stiffened circular steel plates-comparisons between experiment and theory. Comput Struct 1990;37:55–70.

[10] Koizumi M. The concept of FGM. Ceramic Transformer, Funct Graded Mate 1993;34:3–10.

[11] Shen HS. Nonlinear bending response of functionally graded plates subjected to transverse loads and in thermal environments. Int J Mech Sci 2002;44:561–84.

[12] Najafizadeh MM, Eslami MR. Buckling analysis of circular plates of functionally graded materials under uniform radial compression. Int J Mech Sci 2002;44:2479–93.

[13] Jomehzadeh E, Saidi AR, Atashipour SR. An analytical approach for stress analysis of functionally graded annular sector plates. Mater Des 2009;30:3679–85.

[14] Sahraee S. Bending analysis of functionally graded sectorial plates using Levinson plate theory. Compos Struct 2009;88:548–57.

[15] Aghdam MM, Shahmansouri N, Mohammadi M. Extended Kantorovich method for static functionally graded sector plates. Math Comput in Simulation, http://dx.doi.org/10.1016/j.matcom.2010.07.029, in press.

[16] Saidi AR, Hejripour F, Jomehzadeh E. On the stress singularities and boundary layer in moderately thick functionally graded sectorial plates. Appl Math Modeling 2010;34:3478–92.

[17] Nguyen-Xuan H, Rabczuk T, Bordas S, Debongnie JF. A smoothed finite element method for plate analysis. Comput Methods in Appl Mech Eng 2008;197:1184–203.

[18] Nguyen-Xuan H, Liu GR, Thai-Hoang C, Nguyen-Thoi T. An edge-based smoothed finite element method with stabilized discrete shear gap technique for analysis of Reissner–Mindlin plates. Comput Methods Appl Mech Eng 2010;199(9–12):471–89.

[19] Nguyen-Xuan H, Tran LV, Nguyen-Thoi T, Vu Do HC. Analysis of functionally graded plates using an edge-based smoothed finite element method. Compos Struct 2011;93:3019–39.

[20] Nguyen-Xuan H, Tran LV, Thai CH, Nguyen-Thoi T. Analysis of functionally graded plates by an efficient finite element method with node-based strain smoothing. Thin-Walled Struct 2012;54:1–18.

[21] Thai CH, Tran LV, Tran DT, Nguyen-Thoi T, Nguyen-Xuan H. Analysis of laminated composite plates using higher-order shear deformation theory and node-based smoothed discrete shear gap method. Appl Math Modelling 2012;36:5657–77.

[22] Nguyen-Thanh N, Rabczuk T, Nguyen-Xuan H, Bordas S. A smoothed finite element method for shell analysis. Comput Methods Appl Mech Eng 2008;198:165–77.

[23] Nguyen-Thanh N, Rabczuk T, Nguyen-Xuan H, Bordas S. An alternative alpha finite element method free and forced vibration analysis of solids using triangular meshes. J Comput Appl Math 2010;233(9):2112–35.

[24] Nguyen-Thanh N, Rabczuk T, Nguyen-Xuan H, Bordas S. An alternative alpha finite element method with stabilized discrete shear gap technique for analysis of Mindlin–Reissner plates. Finite Elem Anal Des 2011;47(5):519–35.

[25] Hughes TJR, Cottrell JA, Bazilevs Y. Isogeometric analysis: CAD, finite elements, NURBS, exact geometry and mesh refinement. Comput Methods Appl Mech Eng 2005;194:4135–95.

[26] Bazilevs Y, Calo VM, Cottrell JA, Evans JA, Hughes TJR, Lipton S, Scott MA, Sederberg TW. Isogeometric analysis using T-splines. Comput Methods in Appl Mech Eng 2010;199:229–63.

[27] Nguyen-Thanh N, Kiendl J, Nguyen-Xuan H, Wüchner R, Bletzinger KU, Bazilevs Y, Rabczuk T. Rotation free isogeometric thin shell analysis using PHT-splines. Comput Methods in Appl Mech Eng 2011;200:3410–24.

[28] Golmakani ME, Kadkhodayan M. Nonlinear bending analysis of annular FGM plates using higher-order shear deformation plate theories. Compos Struct 2011;93:973–82.

[29] Golmakani ME, Kadkhodayan M. Large deflection analysis of circular and annular FGM plates under thermo-mechanical loadings with temperature-dependent properties. Compos Part B 2011;42:614–25.

[30] Golmakani ME, Kadkhodayan M. An investigation into the thermoelastic analysis of circular and annular FGM plates. Mech Adv Mater Struct, http://dx.doi.org/10.1080/15376494.2012.677101, in press.

[31] Kadkhodayan M, Alamatian J, Turvey GJ. A new fictitious time for the dynamic relaxation (DXDR) method. Int J for Numer Methods Eng 2008;74:996–1018.

[32] Kadkhodayan M, Zhang LC, Sowerby R. Analysis of wrinkling and buckling of elastic plates by DXDR method. Comput Struct 1997;65:561–74.

[33] Zhang LC, Kadkhodayan M, Mai YW. Development of the maDR method. Comput Struct 1994;52:1–8.

[34] Praveen GN, Reddy JN. Nonlinear transient thermoelastic analysis of functionally graded ceramic–metal plates. Int J Solids Struct 1998;35:4457–76.

[35] Nath Y, Sharda HB, Sharma A. Non-linear analysis of moderately thick sector plates. Commun Nonlinear Sci Numer Simul 2005;10:765–78.